(2)

WICK-TYPE LIQUID-METAL COMBUSTION

FINAL REPORT

Grant No. 00014-89-J-1188
(April 15, 1991 to April 14, 1992)

Department of The Navy
Office of Naval Research
800 North Quincy Street
Arlington, Virginia 22217-5000

By

L.-D. Chen and R. C. Damaso

The University of Iowa
College of Engineering
Department of Mechanical Engineering
Iowa City, Iowa 52242

May 1992

WICK-TYPE LIQUID-METAL COMBUSTION

FINAL REPORT

Grant No. 00014-89-J-1188
(April 15, 1991 to April 14, 1992)

Department of The Navy
Office of Naval Research
800 North Quincy Street
Arlington, Virginia 22217-5000

By

L.-D. Chen and R. C. Damaso

The University of Iowa
College of Engineering
Department of Mechanical Engineering
Iowa City, Iowa 52242

May 1992

ABSTRACT

A numerical study is conducted to study lithium-sulfur hexafluoride (Li-SF_6) wick diffusion flames. The objective of this study is to assess the effects of changing the geometry (height H and aspect ratio H/y_o) and ambient conditions (free-stream velocity u_∞ and gravity) on the burning rate and heat transfer. Wick combustion is identified as a boundary-layer gaseous diffusion flame with multiphase combustion products. A mathematical model for wick diffusion flames is established employing a conserved scalar approach. Both forced and mixed convective burning conditions are considered. Laminar, variable-property, boundary-layer equations are cast into dimensionless forms using the modified Howarth-Dorodnitzyn transformation for vertical plates and cylinders. The state relationships for the properties are taken from existing data of Li-SF_6 combustion at a pressure of P = 0.01 MPa.

Forced convective burning, for which the Reynolds number ($Re = u_\infty H/\nu_\infty$) is the important dimensionless parameter, is studied first. The results show that increasing u_∞ increases the total burning rate, $\dot{m}$. A relationship between $\dot{m}$ and Re is obtained for both planar and cylindrical wicks of a given geometry (H = 100 mm, y_o = 12.5 mm). The flat-plate solution yields a fuel mass burning rate per unit surface area (i.e. local fuel burning rate) following the $x^{-1/2}$ dependence of the classical similarity solution, where x is the streamwise distance. This dependence is not evident in the cylinder solution. Cylindrical wick geometries yield enhanced burning rates over planar wicks.

For the case of mixed convective burning, the burning rate results approach either the forced or natural convective burning limits as u_∞ is increased or decreased, respectively. Critical Richardson numbers ($Ri = Gr/Re^2$) specifying these burning limits are determined for the given baseline condition. When the wick height is the only parameter varied, the different curves for the local fuel burning rate, $\dot{m}''$, collapse on one another, if plotted versus the local Richardson number (Ri_x). Reducing gravity results in

a lower burning rate because the influence of natural convection is diminished. Under microgravity conditions (1/1000th of gravity at sea level), mixed convective burning nearly resembles forced convection. The results for cylindrical wicks approach the results for planar wicks as the radius is increased, keeping the height constant. The local fuel burning rates curves for cylindrical wicks of 50.8 and 100 mm (H/y_o = 2 and 1, respectively) deviate slightly from the curve for a flat plate undergoing the same burning conditions. In general, cylindrical wick geometries yield enhanced burning rates over planar wicks.

The major limitation of the present study is that the analysis does not take in account radiative heat transfer, end effects of a finite wick, and the presence of non-condensable gases. Further analysis to account for these effects is recommended.

ACKNOWLEDGEMENT

This work was supported, in aprt, by the Office of Naval Research under Grant No. 00014-89-J-1188 with Dr. Gabriel D. Roy serving as Scientific Officer.

TABLE OF CONTENTS

LIST OF TABLES

LIST OF FIGURES

NOMENCLATURE

Symbol	Description
a_g	arbitrary gravitational constant
C_p	specific heat
D	binary diffusion coefficient
f	dimensionless stream function
g_o	acceleration of gravity
Gr	Grashof number, $Gr = a_g g_o H^3(\rho_\infty/\rho_w - 1)/\nu_\infty^2$
H	plate height
h	heat transfer coefficient
$\bar{h}$	average heat transfer coefficient
h_{fg}	enthalpy of vaporization
k	thermal conductivity
$\dot{m}''$	local fuel burning rate
$\dot{m}$	total fuel burning rate
n	arbitrary constant of geometry (n = 1 for cylinder, n = 0 for flat plate)
Nu_x	Nusselt number, $Nu_x = hx/k_w$
$\bar{Nu}_H$	average Nusselt number, $\bar{Nu}_H = \bar{h}H/k_w$
Pr	Prandtl number
Re	Reynolds number, $Re = \rho_\infty u_\infty H/\mu_\infty$
Ri	Richardson number, $Ri = Gr/Re^2$
Ri_x	Local Richardson Number, $Ri_x = a_g g_o x(\rho_\infty/\rho_w - 1)/u_\infty^2$

Sc	Schmidt number
T	temperature
u	streamwise velocity
v	cross-stream velocity
x	streamwise direction
y	cross-stream direction
Y_i	mass fraction of species i
y_o	radius of cylindrical wick
Z	mixture function
η	similarity variable
μ	dynamic viscosity
ν	kinematic viscosity
ρ	density
ξ	similarity variable
ψ	stream function

Subscripts

cr	critical
F	fuel
fc	forced convection
mc	mixed convection
min	lower integration limit
nc	natural convection
st	stoichiometric conditions
w	wall condition
∞	ambient condition

CHAPTER 1

INTRODUCTION

A novel liquid-metal combustion system involving the reaction of lithium (Li) and sulfur hexafluoride (SF_6) is numerically studied. This system (e.g., see Groff and Faeth, 1978) is unique in that it has a high energy density and a high specific energy and that it yields condensed-phase products under normal operating conditions. The high energy density and high specific energy satisfy the volume and weight requirements of propulsion applications and the condensed-phase product provides a means of closed system operation as desired by deep-sea propulsion vessels; thus the liquid-metal combustion system is ideal for undersea applications.

The present study is a one-year continuation of the research of Chen et al. (1991). This report summarizes the research accomplished following that report; namely, on the computational study of forced convective burning of Li-SF_6 wick diffusion flames.

This Chapter summarizes the literature review and the objectives of the study. The publications resulting from this Navy sponsored research, i.e., Chen et al. (1991) and the present study, include Chen et al. (1990 and 1991), Hsu and Chen (1991 and 1992), Lyu and Chen (1991, 1991a and 1991b), Wu and Chen (1992), Damaso and Chen (1992). Two doctoral dissertations, Lyu (1991) and Hsu (1991), were supported by this Navy sponsored research program; and one additional doctoral dissertation, Wu (1991), and one M. S. thesis, Damaso (1992), were partially supported.

Li-SF_6 Combustion

The reaction of Li and SF_6 follows the stoichiometry:

$$8\,Li + SF_6 \rightarrow 6\,LiF + Li_2S \qquad (1.1)$$

The combustion products (LiF and Li_2S) are soluble in liquid lithium, yielding two immiscible liquids-- fuel-rich and product-rich liquids. The density of the product-rich liquid is heavier than the fuel-rich liquid (and pure Li), allowing for constant volume operation. This system is unique in that it has a high energy density and a high specific energy and that it yields condensed-phase products under normal operating conditions. The high energy density and high specific energy satisfy the volume and weight requirements of undersea propulsion systems, as well as space applications. The condensed-phase product provides a means of closed system operation. Furthermore, Li is stable (non-reacting), and, at room temperature, is in solid phase. SF_6 is non-toxic and stored as a liquid with a high vapor pressure. The high vapor pressure allows the injection of SF_6 into the combustor without the need of a pressurizing device. Li and SF_6 thus make an attractive reaction pair for undersea propulsion and space applications.

One major system configuration already studied is the reactive heat pipe (or wick configuration), e.g. see Lyu et al. (1990) and the references cited therein. When a wick is employed, liquid Li is supplied through capillary action, and the heat transfer is accomplished by evaporation and condensation of Li. While the wick stands vertically during combustion, the buoyancy effects result in natural convective burning along the surface. However, in space applications, where microgravity conditions exist, buoyancy effects may be negligible. This leads to the introduction of forced convective burning, in which a free stream of oxidant (SF_6) is blown past the wick surface to facilitate combustion. One advantage forced convective burning has is that by varying the free stream velocity of the oxidant the fuel burning rate can be changed accordingly, thus,

allowing for changes in heat output of the combustor. Furthermore, forced convective burning is independent of gravity.

Previous Work

Previous work has been done in the area of convective burning and, in particular, natural convective burning. Regarding natural convective burning of Li-SF_6 along a flat plate, Lyu (1991) showed that the local fuel burning rate, $\dot{m}''$, is proportional to $\xi^{-1/4}$, where ξ is the dimensionless streamwise distance. In addition, Lyu obtained similarity solutions for the planar (flat plate) wick geometry, based on a system pressure of 0.01 MPa and wicks of height (H = 100 mm). Cylindrical wick geometries with radius (y_o = 12.5 mm) did not yield similarity solutions. Much of this study is based on Lyu's work and extends it into the realm of forced and mixed convective burning. Regarding forced convective burning, Williams (1985) predicted the local fuel burning rate along a horizontal fuel plate to be proportional to $\xi^{-1/2}$.

Though forced convective burning is ideal for space applications, experimental research is presently confined to earth, where microgravity conditions do not exist. In these experiments, both modes of burning--natural and forced--must be accounted for. Therefore, the study of mixed convective burning gains its significance in relation to space applications. A major challenge is to perform earth-bound experiments (involving mixed convective burning) that approximate conditions found in space. To aid in these experiments, this study presents results regarding mixed convective burning.

This study draws on the work done for natural and forced convective burning, as well as for mixed convection. Jaluria (1986) did a numerical study on aiding mixed convective flow (non-reacting) over a heated vertical surface. The study concluded that natural convection has a major influence in mixed convection. In addition, the study

found that for large values of the mixed convection parameter, $Gr/Re^{5/2}$, the Nusselt number curves approached the results for pure natural convection. Yao (1985) studied mixed convection along a vertical flat plate. Yao's paper stated that natural convection effects are small near the leading edge, and that the forced convection limit is the solution of the problem at the leading edge. Yao also presented results for heat transfer in terms of the Nusselt number.

Objectives

As discussed earlier, the wick-type liquid-metal combustor is of interest due to its use as an energy source for space applications. The overall objective of the present study is to extend the methodology (developed for lithium-sulfur hexafluoride wick diffusion flames under natural convective burning conditions) to investigate forced convective and mixed convective burning of wick diffusion flames. Upon modeling forced and mixed convective burning, numerical solutions are obtained to assess the effects due to geometry (cylinder versus flat plate, wick height, aspect ratio) and physical environment (free-stream velocity of oxidant, gravity) on the wick combustion of Li and SF_6.

Specifically, the objectives of the present study are the following:

(1) To extend the mathematical model developed for wick-type liquid-metal diffusion flames undergoing natural convective burning to flames undergoing mixed convective burning.

(2) To obtain numerical solutions to assess the effects due to geometry (cylindrical versus planar wicks, wick height, aspect ratio) and ambient conditions (free-stream velocity of oxidant, gravity) on the wick combustion of Li and SF_6.

(3) To present results that add to the knowledge of earth-bound combustion experiments performed for varying gravity conditions.

CHAPTER 2

THEORETICAL CONSIDERATIONS

The present study employs a conserved scalar approach for wick diffusion flames. The governing equations and boundary conditions discussed in this chapter are cast into dimensionless forms employing a similarity transformation. The dimensionless parameters or similarity variables are helpful in identifying the physical quantities important to the combustion process.

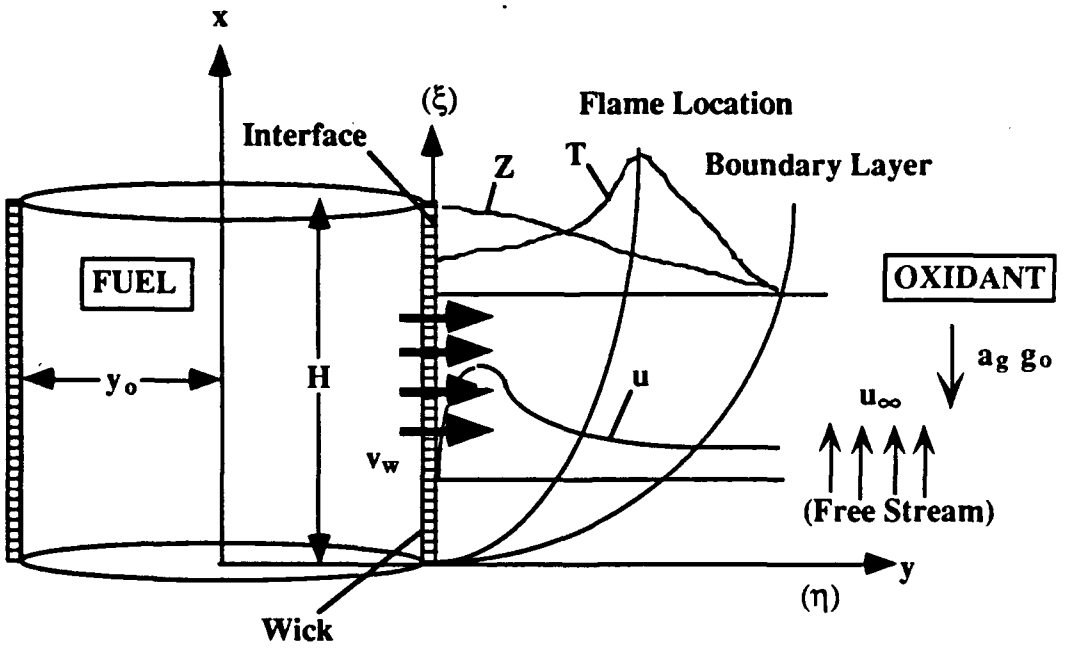

Figure 2-1. The coordinate system.

Governing Equations and Boundary Conditions

The following analysis extends the modeling of Lyu (1991) to account for purely forced convective burning (e.g. that at zero-gravity condition) and mixed convective burning (combined forced and natural convection). Following Lyu et al. (1990), Li-SF_6 wick combustion is assumed as a diffusion flame with infinitely fast chemical reactions. Steady-state, two-dimensional boundary-layer flows are also assumed. Introducing the assumptions of unity Lewis number, identical (binary) diffusion coefficients for all species, no radiative heat loss, negligible viscous dissipation, uniform interface condition, a conserved scalar approach can be employed. Such an approach, which combines the species and energy equations into a single mixture fraction equation, is applied in modeling diffusion flames when locally kinematic (velocity), thermal (temperature), and phase equilibria are established in the flow. In this study, mixture fraction is defined as the effective mass fraction resulting from the fluid supplied through the wick action at any point in the flow field.

Considering the coordinate system illustrated in Figure 2-1, the governing equations are

Continuity:

$$\frac{\partial(\rho u y^n)}{\partial x} + \frac{\partial(\rho v y^n)}{\partial y} = 0 \qquad (2.1)$$

Momentum:

$$\rho u \frac{\partial u}{\partial x} + \rho v \frac{\partial u}{\partial y} = \frac{1}{y^n} \frac{\partial}{\partial y}\left(y^n \mu \frac{\partial u}{\partial y}\right) + a_g g_o (\rho_\infty - \rho) \qquad (2.2)$$

Mixture Fraction:

$$\rho u \frac{\partial Z}{\partial x} + \rho v \frac{\partial Z}{\partial y} = \frac{1}{y^n} \frac{\partial}{\partial y} \left(y^n \rho D \frac{\partial Z}{\partial y} \right) \tag{2.3}$$

where g_o is the gravitational acceleration at sea level, a_g is an arbitrary constant for reduced gravity conditions; e.g. $a_g = 0$ for zero gravity (or pure forced convection) and $a_g = 1$ for normal gravity (or mixed convection). The superscript "n" accounts for different geometries, i.e., n = 0 for flat plates and n = 1 for cylinders. D is the binary diffusion coefficient, and Z is the mixture fraction, i.e., a Shvab-Zeldovich variable (Williams, 1985). The mixture fraction can be viewed as a dimensionless enthalpy (h), or a species concentration (Y):

$$Z = \frac{h - h_\infty}{h_w - h_\infty} = \frac{Y_m - Y_{m\infty}}{Y_{mw} - Y_{m\infty}} \tag{2.3a}$$

Eq. (2.3) uses the conserved scalar, Z, to combine the species and energy equations (Lyu, 1991). The equations for species (2.3b) and energy (2.3c) are

Species:

$$\rho u \frac{\partial Y_m}{\partial x} + \rho v \frac{\partial Y_m}{\partial y} = \omega_m + \frac{1}{y^n} \frac{\partial}{\partial y} \left(y^n \rho D \frac{\partial Y_m}{\partial y} \right) \tag{2.3b}$$

Energy:

$$\rho u \frac{\partial h}{\partial x} + \rho v \frac{\partial h}{\partial y} = \frac{1}{y^n} \frac{\partial}{\partial y} \left(y^n \frac{k}{C_p} \frac{\partial h}{\partial y} \right) \tag{2.3c}$$

Boundary conditions are specified for no-slip walls. Still environments are assigned for natural convection conditions, and parallel flow is assigned for forced and mixed convection.

$x = 0$	$y = 0$	$v = Z = 0.$
	$y \rightarrow \infty$	$u = 0$ (natural convection)
		$u = u_\infty$ (forced and mixed convection)
		$Z = 0$
$0 < x \leq H$	$y = 0$	$u = 0, v = v_w, Z = 1$
$0 < x \leq H$	$y \rightarrow \infty$	$u = 0$ (natural convection)
		$u = u_\infty$ (forced and mixed convection)
		$Z = 0$ (2.4)

where v_w is determined (Lyu, 1991) by the heat and mass balance at the interface, and u_∞ is the free-stream velocity. The formulation presented, i.e., Eqs. (2.1) to (2.4), is for laminar, boundary-layer reacting flows.

Similarity Transformation

The governing equations are cast into a dimensionless form in terms of the stream function and similarity variables, using a modified Howarth-Dorodnitzyn transformation. The transformation has independent variables ξ and η, which are defined as

$$\xi = \frac{x}{H}$$

$$\eta = \left[\frac{u_\infty}{2\xi H \rho_\infty \mu_\infty}\right]^{1/2} \int_{(0 \text{ or } y_o)}^{y} \rho \frac{y^n}{y_o^n} dy \tag{2.5}$$

Momentum Equation

The governing equations are cast into dimensionless form, beginning with the momentum equation, Eq. (2.2). The left-hand side of the equation includes velocities u, v, and their partial derivatives. The u and v terms are defined in terms of the dimensional stream function, ψ, and dimensionless stream function, f.

$$u = \frac{1}{\rho\, y^n} \frac{\partial \psi}{\partial y} \tag{2.6}$$

$$v = -\frac{1}{\rho\, y^n} \frac{\partial \psi}{\partial x} \tag{2.7}$$

where ψ is given as

$$\psi = f\, y_o^n [2\xi H \rho_\infty \mu_\infty u_\infty]^{1/2} \tag{2.8}$$

The partial derivative of ψ with respect to y is

$$\frac{\partial \psi}{\partial y} = \frac{\partial \psi}{\partial \xi}\frac{\partial \xi}{\partial y} + \frac{\partial \psi}{\partial \eta}\frac{\partial \eta}{\partial y} = \frac{\partial \psi}{\partial \eta}\frac{\partial \eta}{\partial y} \tag{2.9}$$

The term $\partial\xi/\partial y$ is zero because ξ is not a function of y. Evaluating the partial derivatives, one obtains

$$\frac{\partial \psi}{\partial \eta} = \frac{\partial f}{\partial \eta} [2\xi H \rho_\infty \mu_\infty u_\infty]^{1/2} y_o^n \tag{2.10}$$

and

$$\frac{\partial \eta}{\partial y} = \left[\frac{u_\infty}{2\xi H \rho_\infty \mu_\infty}\right]^{1/2} \rho \frac{y^n}{y_o^n} \tag{2.11}$$

Substituting Eqs. (2.9), (2.10), and (2.11) into Eq. (2.6), an expression for u is obtained:

$$u = u_\infty \frac{\partial f}{\partial \eta} \tag{2.12}$$

Similarly, an expression for v can be obtained by first taking the partial derivative of ψ with respect to x:

$$\frac{\partial \psi}{\partial x} = \frac{\partial \psi}{\partial \xi}\frac{\partial \xi}{\partial x} + \frac{\partial \psi}{\partial \eta}\frac{\partial \eta}{\partial x} \tag{2.13}$$

or

$$\frac{\partial \psi}{\partial x} = \frac{\partial}{\partial \xi} [f (2\xi H \rho_\infty \mu_\infty u_\infty)^{1/2} y_o^n] \frac{1}{H} + \frac{\partial}{\partial \eta} [f (2\xi H \rho_\infty \mu_\infty u_\infty)^{1/2} y_o^n] \frac{\partial \eta}{\partial x} \tag{2.14}$$

Evaluating Eq. (2.14) and substituting into Eq. (2.7), an expression for v is obtained:

$$v = -\frac{1}{\rho} \frac{y^n}{y_o^n} \left(\frac{\rho_\infty \mu_\infty u_\infty}{2\xi H}\right)^{1/2} \left[f + 2\xi \frac{\partial f}{\partial \xi} + 2\xi H \frac{\partial f}{\partial \xi}\frac{\partial \eta}{\partial x}\right] \tag{2.15}$$

With expressions for u and v derived, $\partial u/\partial x$ and $\partial u/\partial y$ must be derived to complete the evaluation of the left-hand side of the momentum equation, Eq. (2.3). First, the term $\partial u/\partial x$ is found:

$$\frac{\partial u}{\partial x} = \frac{\partial}{\partial x}\left(u_\infty \frac{\partial f}{\partial \eta}\right) \tag{2.16}$$

or

$$\frac{\partial u}{\partial x} = u_\infty \left[\frac{1}{H}\frac{\partial^2 f}{\partial \xi \partial \eta} + \frac{\partial \eta}{\partial x}\frac{\partial^2 f}{\partial \eta^2}\right] \tag{2.17}$$

Then, the term $\partial u/\partial y$ is expressed as

$$\frac{\partial u}{\partial y} = \frac{\partial}{\partial y}\left(u_\infty \frac{\partial f}{\partial \eta}\right) = u_\infty \frac{\partial^2 f}{\partial \eta^2}\frac{\partial \eta}{\partial y} \tag{2.18}$$

or

$$\frac{\partial u}{\partial y} = \rho u_\infty \frac{y^n}{y_o^n}\left[\frac{u_\infty}{2\xi H \rho_\infty \mu_\infty}\right]^{1/2} \frac{\partial^2 f}{\partial \eta^2} \tag{2.19}$$

The terms $u(\partial u/\partial x)$ and $v(\partial u/\partial y)$ can now be evaluated.

$$u\frac{\partial u}{\partial x} = u_\infty 2 \frac{\partial f}{\partial \eta}\left[\frac{1}{H}\frac{\partial^2 f}{\partial \xi \partial \eta} + \frac{\partial \eta}{\partial x}\frac{\partial^2 f}{\partial \eta^2}\right] \tag{2.20}$$

$$v\frac{\partial u}{\partial y} = -\frac{u_\infty^2}{2\xi H}\left[f\frac{\partial^2 f}{\partial \eta^2} + 2\xi\frac{\partial f}{\partial \xi}\frac{\partial^2 f}{\partial \eta^2} + 2\xi H\frac{\partial \eta}{\partial x}\frac{\partial f}{\partial \eta}\frac{\partial^2 f}{\partial \eta^2}\right] \tag{2.21}$$

With the terms on the left-hand side of the momentum equation determined, the focus of attention now turns to the right-hand side. Multiplying Eq. (2.19) (the expression for $\partial u/\partial y$) by y^n and μ, and then taking its derivative with respect to y, one obtains the right-hand side of the momentum equation:

$$\frac{1}{y^n}\frac{\partial}{\partial y}\left(y^n\mu\frac{\partial u}{\partial y}\right) = \frac{1}{y^n}\frac{\partial}{\partial \eta}\left(y^n\mu\frac{\partial u}{\partial y}\right)\frac{\partial \eta}{\partial y} \tag{2.22}$$

and

$$\frac{1}{y^n}\frac{\partial}{\partial y}\left(y^n\mu\frac{\partial u}{\partial y}\right) = \frac{\rho u_\infty^2}{2\xi H}\frac{\partial}{\partial \eta}\left[\frac{\rho\mu}{\rho_\infty\mu_\infty}\left(\frac{y}{y_o}\right)^{2n}\frac{\partial^2 f}{\partial \eta^2}\right] \tag{2.23}$$

The nondimensional form of the momentum equation is nearly complete. Setting the left- and right-hand sides of the momentum equation equal to each other, one obtains

$$\rho u_\infty^2\left[\frac{1}{H}\frac{\partial^2 f}{\partial \xi \partial \eta} + \frac{\partial \eta}{\partial x}\frac{\partial^2 f}{\partial \eta^2}\right]\frac{\partial f}{\partial \eta} - \frac{\rho u_\infty^2}{2\xi H}\left[f\frac{\partial^2 f}{\partial \eta^2} + 2\xi\frac{\partial f}{\partial \xi}\frac{\partial^2 f}{\partial \eta^2} + 2\xi H\frac{\partial \eta}{\partial x}\frac{\partial f}{\partial \eta}\frac{\partial^2 f}{\partial \eta^2}\right]$$

$$= \frac{\rho u_\infty^2}{2\xi H}\frac{\partial}{\partial \eta}\left[\frac{\rho\mu}{\rho_\infty\mu_\infty}\left(\frac{y}{y_o}\right)^{2n}\frac{\partial^2 f}{\partial \eta^2}\right] + a_g g_o(\rho_\infty - \rho) \tag{2.24}$$

Equation (2.24) can be simplified by multiplying both sides by $(2\xi H)/(\rho u_\infty^2)$, and by expressing the first and second derivatives of f (with respect to η) as f' and f'', respectively. The transformed momentum equation becomes

$$\frac{\partial}{\partial\eta}\left(\frac{\rho\,\mu}{\rho_\infty\,\mu_\infty}\left(\frac{y}{y_o}\right)^{2n} f''\right) + ff'' + \frac{2\xi a_g g_o H(\rho_\infty-\rho)}{\rho u_\infty^2} = 2\xi\left(f'\frac{\partial f'}{\partial\xi} - \frac{\partial f}{\partial\xi}f''\right) \tag{2.25}$$

The buoyancy term on the left-hand side can be expressed in terms of Grashof number, Gr, and Reynolds numbers, Re. These dimensionless parameters are defined as

$$Gr = \frac{a_g g_o H^3(\rho_\infty/\rho_w - 1)}{\nu_\infty^2} \tag{2.26}$$

$$Re = \frac{u_\infty H}{\nu_\infty} \tag{2.27}$$

where $\nu_\infty = \mu_\infty/\rho_\infty$. Substituting the expressions for Gr and Re into the buoyancy term, one obtains

$$\frac{2\xi a_g g_o H(\rho_\infty-\rho)}{\rho u_\infty^2} \cdot \frac{(\rho_\infty - \rho_w)/\rho_w}{(\rho_\infty - \rho_w)/\rho_w} \cdot \frac{H^2}{H^2} \cdot \frac{\nu_\infty^2}{\nu_\infty^2} = 2\xi\,\frac{Gr}{Re^2}\,\frac{(\rho_\infty - \rho)/\rho}{(\rho_\infty - \rho)/\rho_w} \tag{2.28}$$

This buoyancy term can be expressed in terms of the Richardson number, which is the ratio of natural to forced convection (buoyancy to inertial forces), and is defined as

$$Ri = \frac{Gr}{Re^2} \tag{2.29}$$

The final form of the transformed momentum equation is

$$\frac{\partial}{\partial\eta}\left(\frac{\rho\,\mu}{\rho_\infty\,\mu_\infty}\left(\frac{y}{y_o}\right)^{2n} f''\right) + ff'' + 2\xi Ri\,\frac{(\rho_\infty - \rho)/\rho}{(\rho_\infty - \rho_w)/\rho_w} = 2\,\xi\left(f'\frac{\partial f'}{\partial\xi} - \frac{\partial f}{\partial\xi}f''\right) \tag{2.30}$$

Mixture Fraction Equation

In a similar fashion, the transformed equation for mixture fraction, Z, can be derived. On the left-hand side of Eq. (2.3), u and v are already known. Taking the derivatives of Z with respect to x and y, one obtains

$$\frac{\partial Z}{\partial x} = \frac{\partial Z}{\partial \eta}\frac{\partial \eta}{\partial x} + \frac{\partial Z}{\partial \xi}\frac{\partial \xi}{\partial x} = \frac{\partial Z}{\partial \eta}\frac{\partial \eta}{\partial x} + \frac{\partial Z}{\partial \xi}\frac{1}{H} \tag{2.31}$$

and

$$\frac{\partial Z}{\partial y} = \frac{\partial Z}{\partial \eta}\frac{\partial \eta}{\partial y} + \frac{\partial Z}{\partial \xi}\frac{\partial \xi}{\partial y} = \frac{\partial Z}{\partial \eta}\left[\frac{u_\infty}{2\xi H \rho_\infty \mu_\infty}\right]^{1/2} \rho \frac{y^n}{y_o^n} \tag{2.32}$$

Upon substituting Eqs. (2.31) and (2.32) and the expressions for u and v, the left-hand side of Eq. (2.3) becomes

$$\rho u \frac{\partial Z}{\partial x} + \rho v \frac{\partial Z}{\partial y} = \rho u_\infty f' \left[\frac{\partial Z}{\partial \eta}\frac{\partial \eta}{\partial x} + \frac{\partial Z}{\partial \xi}\frac{1}{H}\right] -$$

$$\frac{\rho}{\rho}\frac{y^n}{y_o^n}\left(\frac{\rho_\infty \mu_\infty u_\infty}{2\xi H}\right)^{1/2}\left[f + 2\xi\frac{\partial f}{\partial \xi} + 2\xi H \frac{\partial f}{\partial \xi}\frac{\partial \eta}{\partial x}\right] \cdot \frac{\partial Z}{\partial \eta}\left[\frac{u_\infty}{2\xi H \rho_\infty \mu_\infty}\right]^{1/2} \rho \frac{y^n}{y_o^n} \tag{2.33}$$

or

$$\rho u \frac{\partial Z}{\partial x} + \rho v \frac{\partial Z}{\partial y} = \frac{\rho u_\infty}{H} f' \frac{\partial Z}{\partial \xi} - \frac{\rho u_\infty}{2\xi H} f \frac{\partial Z}{\partial \eta} - \frac{\rho u_\infty}{H}\frac{\partial f}{\partial \xi}\frac{\partial Z}{\partial \eta} \tag{2.34}$$

Similarly, the right-hand side terms of Eq. (2.3) can be derived. Multiplying $\partial Z/\partial y$ by y^n, ρ, and D, and then taking the derivative with respect to η, the following equation is obtained:

$$\frac{1}{y^n}\frac{\partial}{\partial y}\left(y^n \rho D \frac{\partial Z}{\partial y}\right) = \frac{1}{y^n}\frac{\partial}{\partial \eta}\left(y^n \rho D \frac{\partial Z}{\partial \eta}\left[\frac{u_\infty}{2\xi H \rho_\infty \mu_\infty}\right]^{1/2} \rho \frac{y^n}{y_o^n}\right)\frac{\partial \eta}{\partial y} \tag{2.35}$$

where the binary diffusion coefficient, D, is expressed in terms of the Schmidt number, Sc, such that

$$D = \frac{1}{Sc}\frac{\mu}{\rho} = \frac{1}{Pr}\frac{\mu}{\rho} \tag{2.36}$$

The unity Lewis number assumption (Sc = Pr) is invoked in the above equation to express D in terms of the Prandtl number, Pr. Substituting this result into Eq. (2.35) and performing some manipulations, the right-hand side of the mixture fraction equation becomes

$$\frac{1}{y^n}\frac{\partial}{\partial y}\left(y^n \rho D \frac{\partial Z}{\partial y}\right) = \frac{\rho u_\infty}{2\xi H}\frac{\partial}{\partial \eta}\left[\frac{\rho \mu}{\rho_\infty \mu_\infty}\frac{1}{Pr}\frac{y^n}{y_o^n}\frac{\partial Z}{\partial \eta}\right] \tag{2.37}$$

The left- and right-hand sides of the mixture fraction equation are equated to obtain the final form of the transformed mixture fraction equation.

$$\frac{\partial}{\partial \eta}\left(\frac{\rho \mu}{\rho_\infty \mu_\infty}\frac{1}{Pr}\left(\frac{y}{y_o}\right)^{2n}\frac{\partial Z}{\partial \eta}\right) + 3 f \frac{\partial Z}{\partial \eta} = 4 \xi \left(f\frac{\partial Z}{\partial \xi} - \frac{\partial f}{\partial \xi}\frac{\partial Z}{\partial \eta}\right) \tag{2.38}$$

The boundary conditions are specified, satisfying the non-slip wall and uniform-flow ambient conditions:

$$\begin{aligned} &\xi > 0 \qquad \eta = 0 \qquad f = f_w,\ f' = 0,\ Z = 1 \\ &\qquad\qquad \eta \to \infty \qquad f' = 1,\ Z = 0. \end{aligned} \tag{2.39}$$

The solution at $\xi = 0$ is found by setting ξ to zero for the right-hand sides of Eqs. (2.25) and (2.38). Similarity solutions are obtained at $\xi = 0$.

Fuel Burning Rate

An expression for the fuel burning rate per unit surface area can be derived from the expression (see Lyu, 1991) for the wall velocity, v_w,

$$v_w = \frac{k_w}{\rho_w c_{pw}} \frac{1}{Y_{Fw} - 1} \frac{\partial Y_{Fw}}{\partial Z} \frac{\partial Z}{\partial \eta} \frac{\partial \eta}{\partial y}\bigg|_w \tag{2.40}$$

where $\left(\frac{\partial \eta}{\partial y}\right)_w$ is evaluated by

$$\frac{\partial \eta}{\partial y}\bigg|_w = \rho_w \left[\frac{u_\infty}{2\xi H \rho_\infty \mu_\infty}\right]^{1/2} \tag{2.41}$$

Substituting the above equation into Eq. (2.40), v_w becomes

$$v_w = \frac{k_w}{\rho_w c_{pw}} \frac{1}{Y_{Fw} - 1} \frac{\partial Y_{Fw}}{\partial Z} \frac{\partial Z}{\partial \eta} \rho_w \left[\frac{u_\infty}{2\xi H \rho_\infty \mu_\infty}\right]^{1/2}. \tag{2.42}$$

The term $\left[\frac{u_\infty}{2\xi H \rho_\infty \mu_\infty}\right]$ is multiplied by $\frac{H}{H}$ and $\frac{\rho_\infty}{\rho_\infty}$ to yield an expression that includes the Reynolds number, Re, based on height H. The equation for the local fuel burning rate then becomes

$$\dot{m}'' = \rho_w v_w = \frac{1}{\sqrt{2}H} \frac{\rho_w k_w}{\rho_\infty C_{pw}} \frac{1}{Y_{Fw} - 1} \left(\frac{Re}{\xi}\right)^{1/2} \frac{\partial Y_{Fw}}{\partial Z} \frac{\partial Z}{\partial \eta}\bigg|_{\eta=0} \tag{2.43}$$

The local fuel burning rate is integrated over the entire wick surface to obtain the total fuel burning rate, given by the following equation:

$$\dot{m} = H(1) \int_\xi \dot{m}'' \, d\xi \tag{2.44}$$

where the surface area considered is the product of the height H and unity (1), regardless of geometry. This is done so that the total fuel burning rates for both cylindrical and planar wicks can be compared.

Heat Transfer

In addition to the fuel burning rate, an important parameter to heat transfer is the Nusselt number, Nu. The local Nusselt number is defined as

$$Nu_x = \frac{h\,x}{k_w} \tag{2.45}$$

where h is the convective heat transfer coefficient. The convective heat transfer coefficient is obtained by assigning a characteristic temperature difference which, in the

present study, is defined to be T_{st}-T_w, where T_{st} is the stoichiometric temperature and T_w is the wall temperature. The heat transfer rate is obtained by multiplying the enthalpy of fuel vaporization, h_{fg}, with the fuel mass burning rate, $\dot{m}$. The heat transfer coefficient can then be defined as

$$h = \frac{\dot{q}/A}{\Delta T} = \frac{\dot{m}'' h_{fg}}{T_{st}-T_w} \tag{2.46}$$

where $\dot{m}''$ is the fuel burning rate per unit surface area. The local Nusselt number is

$$Nu_x = \frac{\dot{m}'' h_{fg} \xi H}{k_w (T_{st}-T_w)} \tag{2.47}$$

The average Nusselt number, $\bar{N}u_H$, over the surface of the wick is defined by

$$\bar{N}u_H = \frac{\bar{h} H}{k_w} \tag{2.48}$$

where $\bar{h}$ is the average convective heat transfer coefficient:

$$\bar{h} = \frac{1}{A_s} \int_{A_s} h \, dA_s \tag{2.49}$$

In general. the wick surface, A_s, is expressed as

$$A_s = H (2\pi y_o)^n \int_{\xi} d\xi = H (2\pi y_o)^n \cdot 1 \tag{2.50}$$

where n is 0 for a flat plate and 1 for a cylinder. The derivative of A_s is taken with respect to ξ to obtain an expression for dA_s:

$$dA_s = H\,(2\pi y_o)^n\,d\xi \tag{2.51}$$

Equations (2.46), (2.50), and (2.51) are substituted into Eq. (2.49):

$$\bar{h} = \frac{1}{H\,(2\pi y_o)^n} \int_{\xi} \frac{\dot{m}''\,h_{fg}}{T_{st}-T_w} H\,(2\pi y_o)^n\,d\xi \tag{2.52}$$

Simplifying Eq. (2.52), one obtains

$$\bar{h} = \frac{h_{fg}\,H}{H\,(T_{st}-T_w)} \int_{\xi} \dot{m}''\,d\xi \tag{2.53}$$

or

$$\bar{h} = \frac{\dot{m}\,h_{fg}}{H\,(T_{st}-T_w)} \tag{2.54}$$

Finally, substituting Eq. (2.54) into (2.48), one obtains the expression for the average Nusselt number:

$$\bar{Nu}_H = \frac{\dot{m}\,h_{fg}}{k_w\,(T_{st}-T_w)} \tag{2.55}$$

CHAPTER 3

NUMERICAL SOLUTION PROCEDURE

This chapter describes the procedure used to obtain numerical solutions to the governing equations. The procedure is centered around a computer program that solves the transformed governing equations. The code requires that the state relationship for Li-SF_6 combustion be specified. The computer program used in this study was modified from Lyu (1991) to handle mixed convective burning.

To obtain solutions to the governing equations, the state relationship, e.g. $\rho = \rho(Z)$, must be specified. The state relationship was obtained from the equilibrium calculation employing the NASA code with thermodynamic properties of Li_2S estimated from Groff (1976). As one example, the state relationships for temperature and density, taken from Lyu (1991), are shown in Figure 3-1. (The reader should note that the figures are at the end of the chapter.) All the state relationships used in the flow calculations are tabulated in Appendix A, c.f. Table A-1. Note that the interface temperature corresponds to $Z = 1$. These state relationships are based on the converged interface condition ($P = 0.01$ MPa, $Y_{Fw} = 0.38$), and are used in the present study to obtain the fuel burning rates at 0.01 MPa.

The flow calculation program used by Lyu (1991), which is for natural convective burning, was modified to account for forced convective burning, following the approach of Chen and Faeth (1981). The modifications to Lyu's code underwent several steps. First, the code was converted to pure forced convective burning. Gravity was no longer considered (i.e., $a_g = 0$). Certain coefficients in the transformed governing equations were changed, as well as the boundary conditions. The program was tested for a flat

plate, using constant properties and neglecting wall blowing effects. The Blasius solution was obtained, as shown in Figure 3-2.

The code was then modified to handle mixed convective burning. A listing of the FORTRAN computer code is included in Appendix A. The flow calculation program utilizes a finite difference scheme (Keller box method) in solving the governing equations at specified boundary conditions (Cebeci and Bradshaw, 1977). A marching procedure is used to obtain the solution along the streamwise distance. The computation employs 82 and 600 nodal points in the η and ξ directions, respectively. Variable grid sizes are used for both directions. The first 100 ξ grid points are spaced 1×10^{-5} apart, and then spaced 2×10^{-3} apart for the remaining 500 grid points. The η grid points are separated by a value $\Delta\eta$, which grows with each successive grid generated; each successive value of $\Delta\eta$ is multiplied by a factor of 1.05 as the grid is generated from the surface (i.e., $\eta_0 = 0$, $\eta_1 = 1 \times 10^{-2}$, $\Delta\eta_2 = 1.05 \cdot 1 \times 10^{-2}$, $\Delta\eta_3 = 1.05^2 \cdot 1 \times 10^{-2}$, ... , $\Delta\eta_i = 1.05^{i-1} \cdot 1 \times 10^{-2}$). This allows for a more dense grid near the surface and a less dense grid farther from the surface.

In the process of achieving grid independence, the nodal mesh required refinement due to the results of the calculations for the local fuel burning rate; the results shows some peculiarities. Specifically, instead of decreasing "uniformly" along the distance of the surface, the local fuel burning rate showed a "stepping" decrease along the streamwise distance. Figure 3-3 illustrates the stepping phenomenon in more detail. Further investigation of the stepping change found that, in the equation for the local fuel burning rate, the gradient of the mixture fraction was fluctuating.

The stepping change was reduced when the grid size along the wick surface was refined. Figure 3-4 shows the results of how varying the grid size in the ξ direction affects the mixture fraction gradient at the wall, $Z'|_w$, which consequently affects the value for the local fuel burning rate; refer to Eq. (2.43). Four grid sizes were

investigated, corresponding to 254, 504, 600, and 1000 nodal points in the ξ-direction. The first case, which used 254 nodal points in ξ-direction, is the same grid Lyu (1991) used. The first five grid points were variably spaced, while the remaining 249 grid points were spaced 4×10^{-3} apart, beginning at $\xi = 4 \times 10^{-3}$. Since the stepping changes seemed more pronounced near the leading edge ($\xi < 1 \times 10^{-3}$) and since the boundary layer thickness changes more rapidly near the leading edge, more attention was given to this area of the domain. In the second case for 504 nodal points, sizes of the first four grids (first five nodal points) were reduced to one-fourth the size of those in the first case. Beginning at $\xi = 1 \times 10^{-3}$, the remaining 500 nodal points were spaced uniformly by a distance of 2×10^{-3}. The third case involved dividing the region of $\xi < 1 \times 10^{-3}$ into 99 grids of size 1×10^{-5} (100 nodal points). Finally, in the fourth case, 1000 nodal points were employed: 500 nodal points spaced 2×10^{-6} apart ($\xi < 1 \times 10^{-3}$) and 500 nodal points spaced 2×10^{-3} apart ($\xi > 1 \times 10^{-3}$).

The error in calculating the local fuel burning rates can be estimated from the results for $Z'|_w$. For the case of forced convective burning (Re = 3800) along a flat plate, the fluctuation ranges from a minimum of -1.7 to a maximum of -1.85, resulting in a maximum difference of about 8%. The results are shown in Figure 3-5. The maximum fluctuation occurred immediately after $\xi = 0.001$, where the grid spacing jumped from 1×10^{-5} to 2×10^{-3}. The fluctuation can be damped out by refining the grid. In using 2000 grid points with variable grid spacing ($\Delta\xi_n = 1.005 \cdot \Delta\xi_{n-1}$), Figure 3-6 shows little variation in Z' at the wall. Indeed, the value for Z' at the wall and $\dot{m}''$ are sensitive to the grid scheme used, but the total fuel burning rate, $\dot{m}$, is not effected after grid independence is achieved. The calculated total fuel burning rates for the cases of 600 and 2000 grid points differed by less that 1%.

The total fuel burning rates were obtained by performing a numerical integration of the local values along the surface, from ξ_{min} to 1, using Eq. (2.44). Simpson's rule was

used for the integration (Weltner et al., 1986). The total fuel burning rate was calculated for different values of ξ_{min}. The lower integration limit was chosen to be 10^{-4}, using the results shown in Figure 3-7 for forced convective burning along a flat plate. Between $\xi_{min} = 10^{-3}$ and 10^{-4}, there is a 0.42% change. A 0.26% change occurs between 10^{-4} and 10^{-5}.

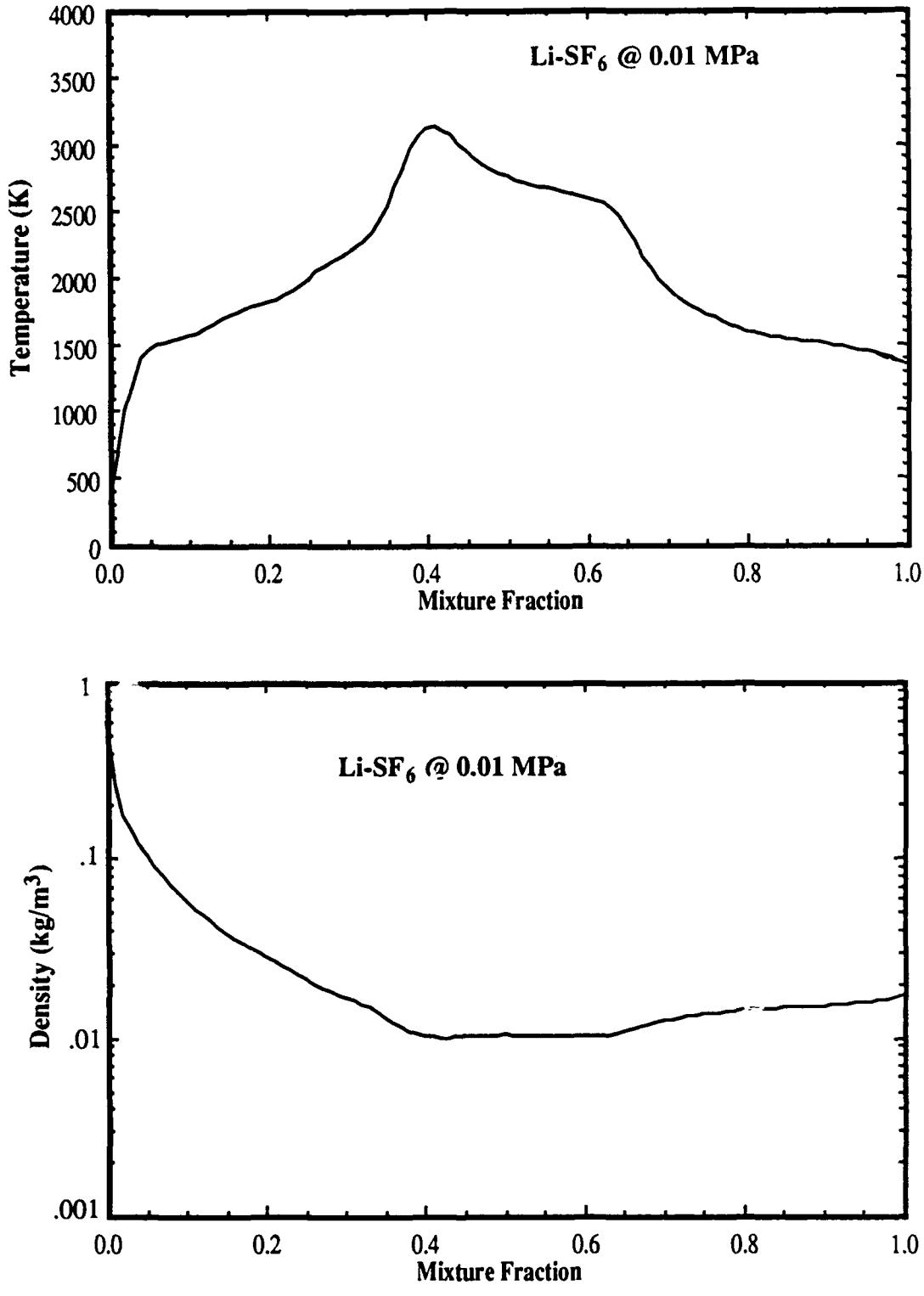

Figure 3-1. State relationship of temperature and density of Li-SF_6 wick combustion $Y_{Fw} = 0.38$, taken from Lyu (1991).

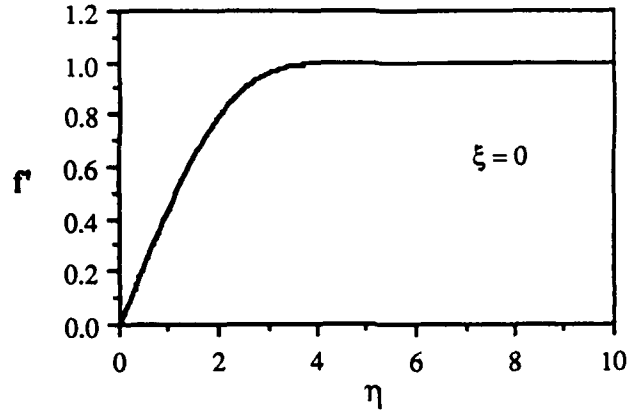

Figure 3-2. Blasius solution.

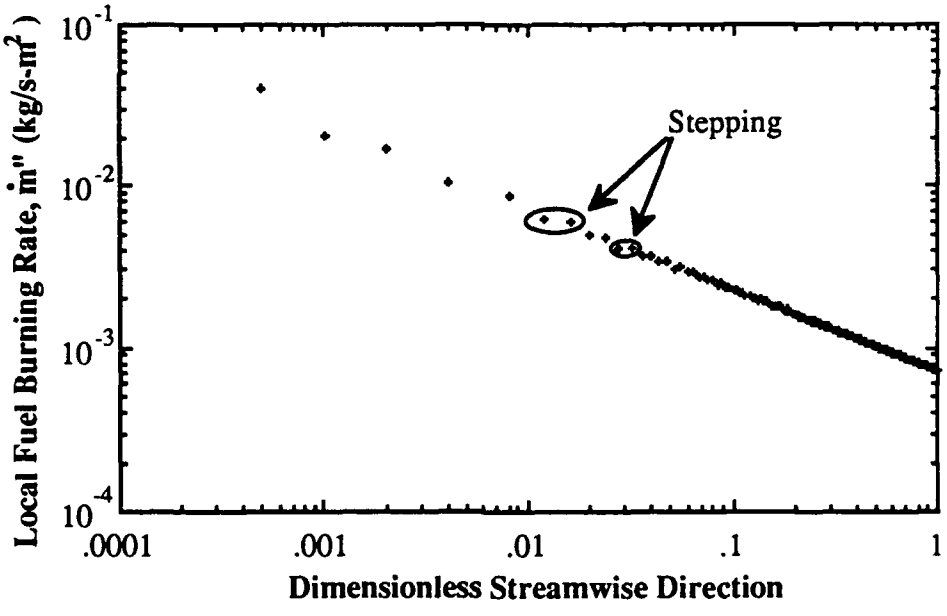

Figure 3-3. Stepping phenomena illustrated: local fuel burning rate along planar wick surface, forced convective burning, Re=3800 (u_∞=1 m/s, H=100 mm, a_g = 0).

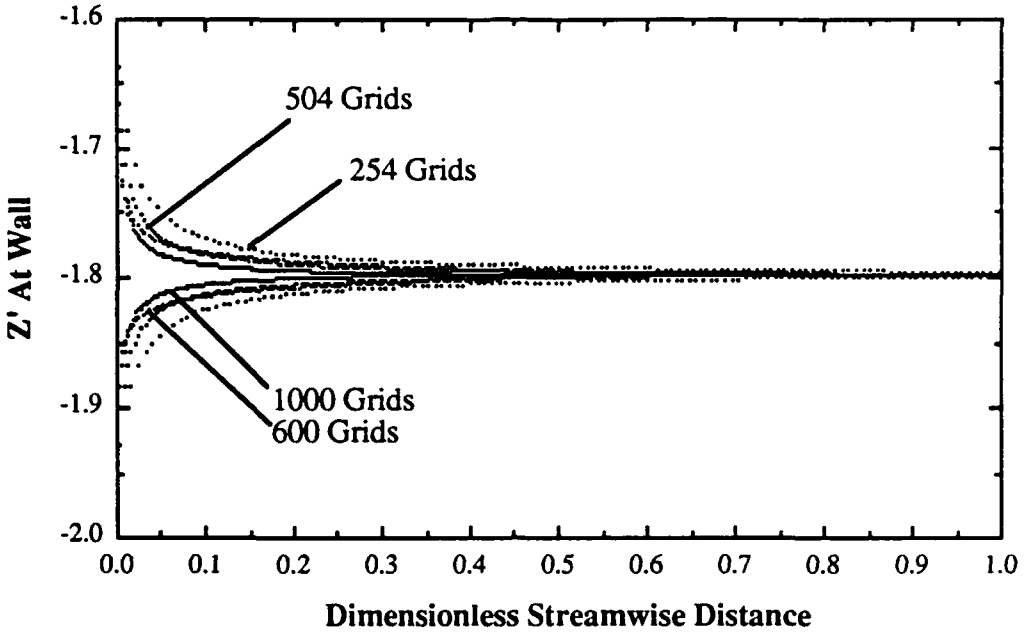

Figure 3-4. Fluctuations of mixture fraction gradient at the wall for various grid schemes: 254, 504, 600, 1000 nodal points (ξ-direction).

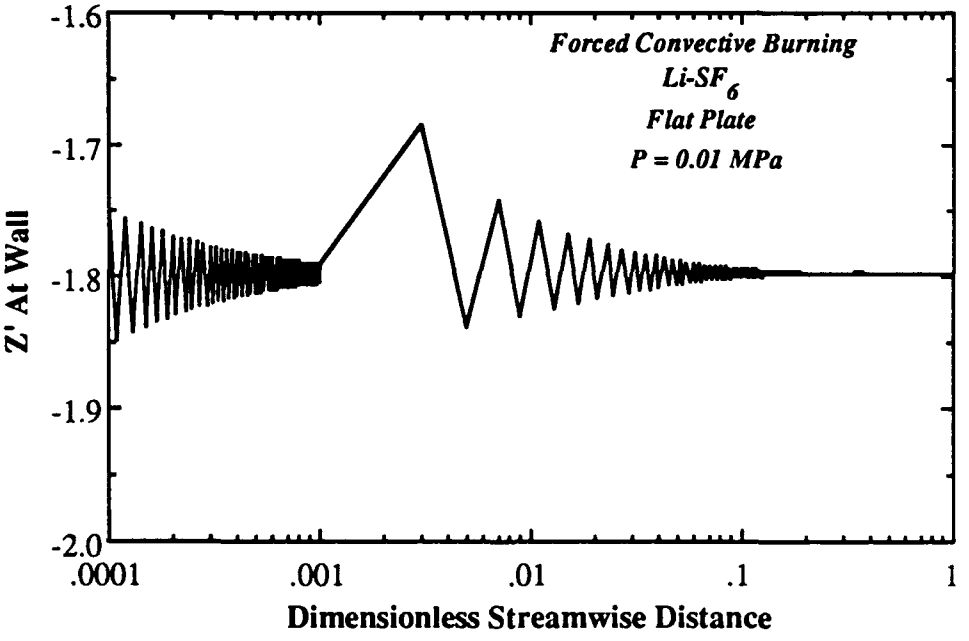

Figure 3-5. Semi-log plot of fluctuation of mixture fraction gradient at the wall, forced convective burning along a flat plate, Re=3800; 600 nodal points (ξ-direction).

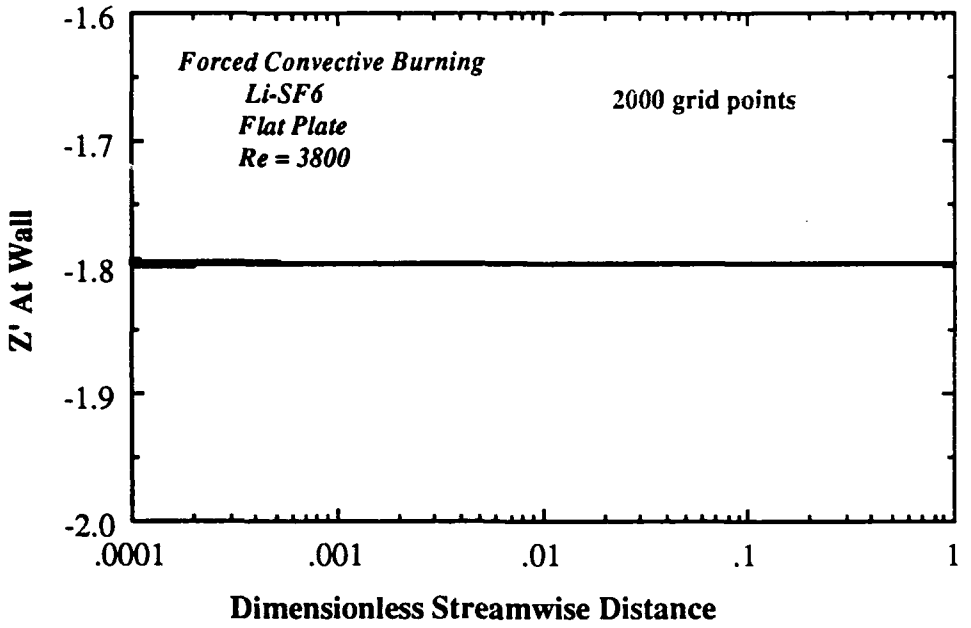

Figure 3-6. Semi-log plot of fluctuation of mixture fraction gradient at the wall, forced convective burning along a flat plate, Re=3800; 2000 nodal points (ξ-direction).

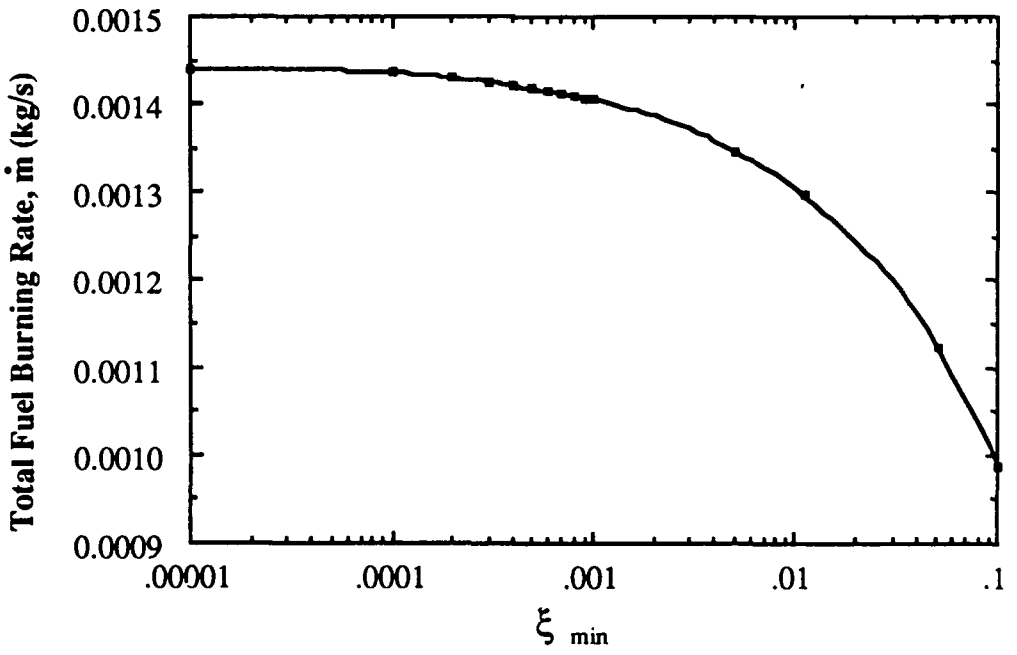

Figure 3-7. Determination of minimum integration limit from total fuel burning rate.

CHAPTER 4

RESULTS AND DISCUSSION

Though presenting the results for mixed convective burning is the main objective of this study, examining forced convective burning offers valuable insight into mixed convective burning. Through a parametric study, this chapter examines forced and mixed convective burning of Li-SF_6 wick diffusion flames. Both wick geometry and ambient conditions are examined for their effects on burning rates. Cylindrical wick geometry is emphasized, since it yields enhanced burning rates. The parameters varied in the study of mixed convective burning are the free-stream velocity of the SF_6 oxidant (u_∞), the wick height (H), the gravity (a_g), and the aspect ratio (height/radius).

Forced Convective Burning

Mixed convective burning combines both natural and forced convection. To develop a better understanding of mixed convection, one may view its components separately, investigating the burning characteristics associated with each component. In this section, the results for forced convective burning ($a_g = 0$) are presented for both planar and cylindrical geometries. In the study of forced convective burning, the parameter subject to variation is the free-stream velocity, u_∞; however, the results are in terms of the Reynolds number, as defined by Eq. (2.27), based on the wick height, H. Other parameters, such as wick height and gravity, remain constant in the study. The wick height is 100 mm, and a_g is 0. For cylindrical wicks, the radius is fixed at 12.5 mm. The system pressure considered in the computation is 0.01 MPa. The state relationships

and interface condition were obtained from Lyu (1991). The interface had a lithium mass fraction of 0.38 and a temperature of 1340 K.

Local fuel burning rates for planar and cylindrical wick diffusion flames are calculated by Eq. (2.43). The results are presented in Figures 4-1 and 4-2 for Re ranging from 3800 (u_∞ = 1 m/s) to 190,000 (50 m/s). A $\xi^{-1/2}$ dependence is observed for the planar case. The results for the cylindrical case deviate from the $\xi^{-1/2}$ dependence, however, due to the curvature effects. The fuel burning rates for natural convective burning (flat plate and cylinder) under the same ambient and geometry conditions (i.e., P = 0.01 MPa, H = 100 mm, and y_o = 12.5 mm) are also graphed for comparison. In contrast to forced convective burning, natural convective burning of a Li-SF_6 wick diffusion flame shows a $\xi^{-0.25}$ dependence for flat plates and a $\xi^{-0.18}$ dependence for cylinders (Lyu, 1991).

The $\xi^{-1/2}$ dependence is typical for the heat and mass transfer across laminar forced convection boundary layers (Williams, 1985). For wick diffusion flames, the $\xi^{-1/2}$ dependence of v_w is a sufficient and necessary condition for the right-hand side of Eqs. (2.30) and (2.38) to vanish, i.e. f_w = constant. The mathematical derivations are included in Appendix B. The solution yields similar profiles for f, f', f'', Z, and Z' at different streamwise locations when the similarity variables are employed. Figure 4-3 shows a representative sample of similarity profiles of the dimensionless streamwise velocity, f'.

When curvature effects are considered, an additional factor, $(y/y_o)^2$, appears in the diffusional transport term. The local fuel burning rates of cylinders deviate from the $\xi^{-1/2}$ dependence of flat plates for $\xi > 0.001$. Similarity solutions are not obtained in the case of the cylindrical wick due to the curvature term. Overall, the fuel burning rates for the cylinder are slightly higher than those for the flat plate. According to Lyu and Chen (1991), under natural convective burning conditions the curvature effect on $\dot{m}''$ becomes important when $y_o \ll H$, or when needle-type cylinders are considered. In addition, as the

cylinder's radius is increased (keeping the height constant) $\dot{m}''$ is observed to approach the flat plate solutions. For example, when the cylinder radius y_o increased to 50.8 mm (H = 100 mm), the local fuel burning rate of an ethanol-air wick diffusion flame approaches that of a planar geometry (Lyu and Chen, 1991). Similar behavior is observed in the present study of Li-SF_6 wick diffusion flames. Using the same wick dimensions as Lyu and Chen (1991), the total fuel burning rates for Li-SF_6 cylindrical wick diffusion flames under forced convection conditions approach the results of a flat-plate wick geometry.

The total fuel burning rates, $\dot{m}$, were calculated using the corresponding local fuel burning rates calculated for various Re. This was done by performing a numerical integration over the height of the wick surface. As discussed earlier, Simpson's rule was used (Weltner et al., 1986), with the lower integration limit, ξ_{min}, set at 0.0001. The results for the planar and cylindrical cases are shown in Figure 4-4. The total fuel burning rates for the cylindrical flames are higher than those for the flat plate flames; $\dot{m}$ is proportional to $Re^{0.5}$ and $Re^{0.33}$ for the flat plate and cylinder, respectively. These relationships are true for the parameters specified. The total burning rate's dependence on Re changes if a different wick geometry is considered.

Mixed Convective Burning

The results from the previous section are for pure forced convective burning, i.e., $a_g = 0$; buoyancy effects are neglected, and Gr is set to zero. In reality, however, low gravity can be expected even in experimental conditions, such as in a space station, where typically $0 < a_g < 0.01$. Furthermore, during the technology development for liquid-metal wick burners, buoyancy effects will be present in earth-bound experiments. At these conditions, mixed convective burning needs to be examined, as to extrapolate the data base for space applications.

The following section examines the effects of changing particular parameters on mixed convective burning. These parameters are the free-stream velocity (u_∞), the wick height (H), the arbitrary gravitational constant (a_g), and the aspect ratio (H/y_0). The results for changing the free-stream velocity are expressed in terms of Richardson number, Ri, instead of u_∞, for sake of clarity. The effects on the burning rates and heat transfer for both cylindrical and planar wick geometries will be highlighted.

Free-stream Velocity

Mixed convection combines both natural and forced convection. The important parameter used in mixed convection is the Richardson number (Ri), which is the ratio of natural to forced convection. As stated earlier in Eq. (2.29), Ri is defined as

$$Ri = \frac{Gr}{Re^2}$$

Ri can be stated more simply by considering the definitions of Gr and Re and then dividing and eliminating terms. The following expression for Ri is obtained:

$$Ri = \frac{a_g g_0 H}{u_\infty^2}\left(\frac{\rho_\infty}{\rho_w} - 1\right) \tag{4.1}$$

From Eq. (4.1) one can notice that Ri decreases as u_∞ is increased by a power of 2. In this computation, the other parameters are fixed ($a_g = 0$ and $H = 100$ mm).

In mixed convective burning, forced and natural convection take turns dominating along the height of the plate. Near the leading edge, forced convection dominates. Figures 4-5 and 4-6 illustrate this phenomenon using the dimensionless streamwise velocity profiles (f' vs. η). At $\xi = 0$ of a flat plate, the maximum velocity is the free-

stream velocity for Ri = 34 (u_∞ = 1 m/s). But as the flow moves downstream, buoyancy effects come into play. The maximum velocity increases as ξ increases, since the buoyancy forces are in the same direction as the flow. At the trailing edge the peak velocity is almost six times the free-stream velocity. The trends are similar to those obtained for aiding mixed convection flow over a vertical surface (Jaluria, 1986). These trends are also observed in the case of the cylinder. The peak velocity at ξ = 1 is over five times greater than the free-stream velocity.

Burning Rates

Results for the local fuel burning rates ($\dot{m}''$) show that, as Ri approaches zero ($u_\infty \rightarrow \infty$), the results approach those for forced convective burning. Figures 4-7 and 4-8 show the results for natural, forced, and mixed convective burning along planar and cylindrical wicks, respectively. The flat plate results suggest that there exists a critical Ri beyond which $\dot{m}''$ approaches the $\xi^{-1/2}$ dependence in the near-leading edge region, or $\xi <$ 0.01, and approaches the $\xi^{-1/4}$ dependence for $\xi \geq 0.01$. The Grashof number, Gr, defined by Eq. (2.26), remains the same (Gr = 4.93 x 10^8) for all the cases involving mixed convection. The total fuel burning rates for the burning curves of Figures 4-7 and 4-8 were calculated, and the results are shown in Figure 4-9. Overall, the values for the cylinder are greater than those for the flat plate. The decrease in the total fuel burning rate ($\dot{m}$) as Ri increases is due to the diminishing contribution of forced convection. As mentioned earlier, Ri increases as u_∞ decreases. For forced convective burning, the total fuel burning rate decreases as u_∞ decreases. Furthermore, the total fuel burning rates for mixed convective burning are higher than those for forced convective burning. As an example, for u_∞ = 10 m/s (cylinder), $\dot{m}_{mc}$ is 7.4 x 10^{-4} kg/s, compared to 6.9 x 10^{-4} kg/s for $\dot{m}_{fc}$.

The question of whether the results for forced and natural convective burning can be used to approximate mixed convective burning is answered by the results tabulated in Table 4-1. As the previous figures showed, for the region near the leading edge, the mixed convective burning curve approaches that of forced convective burning. For the region closer to the trailing edge, the curve approaches that of natural convective burning. One may think that an additive relationship among the different modes of burning might exist; that is, $\dot{m}_{mc} = \dot{m}_{fc} + \dot{m}_{nc}$. The burning rate calculations summarized in Table 4-1, however, indicate that such an additive relationship does not exist.

Despite the fact that an additive relationship does not exist among the burning rates, for certain "critical" values of Ri, mixed convective burning can be approximated as either forced or natural. These critical values of Ri are found by plotting the ratio of fuel burning rates (natural-to-mixed and forced-to-mixed) versus Ri for cylindrical and planar wicks. This is done in Figures 4-10 and 4-11. For a planar wick of height 100 mm, Ri_{cr} is 0.013 for forced convective burning and 155 for natural convective burning. Likewise, for a cylindrical wick of height 100 mm and radius 12.5 mm, Ri_{cr} is 0.028 for forced convective burning and 160 for natural convective burning. The critical Ri for natural convective burning found in this study agrees with other work done. Using a 1% criterion to compare Nu for natural and mixed convection, Yao (1985) determined the value for $Ri_{cr,nc}$ to be 500--the same order of magnitude as the one determined in this study--for a semi-infinite vertical flat plate undergoing mixed convection heat transfer. These results are intended to assist those performing earth-bound experiments related to space applications. For the given geometry (H = 100 mm and y_o = 12.5 mm), the total fuel burning rate for forced convective burning can be approximated using the results from mixed convective burning at the critical Richardson number, $Ri_{cr,fc}$, with an uncertainty of 1%. These critical Ri change when considering different wick sizes.

Heat Transfer

In terms of heat transfer and the local Nusselt number, Nu_x, the results can be represented using Eq. (2.45). The value of Nu_x is based on the difference of the temperatures at the wall (1340 K) and at stoichiometric conditions (3120 K); refer to Figure 3-1. The results are presented graphically in Figures 4-12 and 4-13. Equation (2.45) shows that Nu_x is proportional to ξ to some power, which depends on the relationship between the local fuel burning rate and ξ. For forced convective burning, in which $\dot{m}''$ is proportional to $\xi^{-1/2}$, Nu_x is proportional to $\xi^{1/2}$. Similarly for natural convective burning, in which $\dot{m}''$ is proportional to $\xi^{-1/4}$, Nu_x is proportional to $\xi^{3/4}$. For the case of the flat plate (Figure 4-12), such relationships can be seen. For the curve (Ri = 0.013, forced convection dominant), the slope is approximately 1/2. For Ri = 115, natural convection dominates near the trailing edge, where the burning curve has a slope of approximately 3/4. This observation on the calculated Nusselt number agrees with that of Yao (1985), which stated that in mixed convection the buoyancy force accelerates the flow near the surface and consequently thins the boundary-layer; thus, a higher heat transfer rate is obtained at downstream locations. The average Nusselt numbers, defined by Eq. (2.55) are calculated and the results are shown in Figure 4-14. Similar to the total burning rates, the average Nusselt numbers increase as Ri decreases.

Already being investigated as a heat source in undersea propulsion systems (Hughes et al., 1983, and Lyu et al., 1990), Li-SF_6 wick combustion has the potential of being used in space applications. For instance, the auxiliary power generation system for the Space Station could utilize a combustor consisting of a number of cylindrical wicks undergoing forced convective burning. The heat output could be controlled by either varying the free-stream oxidant velocity or changing the number of wicks used. For the first case in which u_∞ is varied, a relationship between the heat output (per wick) and Re needs to be determined. Such a relationship has been determined already for a cylindric

wick considered in this study (H = 100 mm and y_o = 12.5 mm). For the second case, in which the wick dimensions and free-stream velocity are fixed, the heat output of a cylinder needs to be calculated. Consider, for example, one cylindrical wick (0.1 m in height, 0.0125 m in radius) under forced convective burning conditions (P = 0.01 MPa, u_∞ = 10 m/s). The predicted total fuel burning rate for this case is 5.4 x 10^{-6} kg/s. If one kilogram of Li is assumed to yield 57,400 kJ of energy (Lyu, 1991), then the heat output of one cylinder is 0.31 kW. A power system requiring a 5-kW heat source would need 17 of these wicks considered.

Wick Height

It would be of interest to see how the fuel burning rates vary with changes in wick height. The previous calculations have been based on a wick height of 100 mm. When considering mixed convective burning along wicks of different heights, one must keep in mind the appropriate length scales. Because of this, the results for the local fuel burning rates are plotted versus the local Richardson number, Ri_x, which is defined as

$$Ri_x = \frac{a_g g_o \xi H}{u_\infty^2}\left(\frac{\rho_\infty}{\rho_w} - 1\right) \tag{4.2}$$

instead of the dimensionless streamwise distance, ξ. Figures 4-15 and 4-16 show this trend for local fuel burning rates. For both planar and cylindrical wick geometries, the burning curves overlap one another, unlike the previous cases. The curve for the shortest height (H = 0.01 m) corresponds to the lowest range of local Richardson numbers--roughly, less than Ri_x = 1. The curve for H = 0.1 m spans across the highest range of Ri_x. When the total fuel burning rates are calculated for the given range of heights, a relationship is observed between $\dot{m}$ and Ri. For the flat plate, $\dot{m}$ is proportional to $Ri^{0.71}$.

For the cylinder, $\dot{m}$ is proportional to $Ri^{0.77}$. Figure 4-17 shows the total fuel burning rates. These relationships are limited to the conditions considered (u_∞ = 1 m/s, a_g = 1, y_o = 12.5 mm) and are expected to change for different conditions. The graph indicates that increasing the wick height (greater Ri) increases the total fuel burning rate. This is to be expected since a taller wick means more surface area, thus, a higher burning rate. Furthermore, cylindrical wicks are observed to yield higher total burning rates over planar wicks.

Gravity

The effect of gravity on mixed convective burning is studied by varying the value of a_g. The gravity conditions are changed by setting a_g at a value between 0 and 1; i.e., $0 \leq g \leq g_o$, where g_o is the gravity at sea level. The burning rate calculations are performed for a_g = 1, 0.5, 0.1, 0.01, and 0.001. Typical gravity in an environment like the Space Station would have an a_g of less than 0.01. In the calculations, the other parameters, H (100 mm) and u_∞ (1 m/s), remain fixed. The local fuel burning rates for flat plate and cylinders are presented in Figure 4-18 and 4-19. The curves for natural and forced convective burning are also graphed for comparison. Since gravity is a parameter that affects natural convection only, the local fuel burning rates are approximately the same near the leading edge ($\xi < 0.001$), where forced convection dominates. Moving downstream, the curves diverge; the curves corresponding to smaller values of a_g approach the forced convective burning limit because the relative influence of natural convection diminishes. The buoyancy forces are not as strong because of the decrease in gravity.

The total fuel burning rates for planar and cylindrical Li-SF_6 wick combustion are calculated and presented in Figure 4-20. As expected, the total fuel burning rates are

higher for cylindrical wick geometries than for planar wicks. Overall, for mixed convective burning with variable gravity conditions, the values of $\dot{m}$ approach those for forced convective burning. At $a_g = 0.001$, the total fuel burning rate is 1.46×10^{-3} kg/s (flat plate) and 3.41×10^{-3} kg/s (cylinder); the corresponding total fuel burning rates for forced convective burning are 98.4% (flat plate) and 99.6% (cylinder) of their corresponding mixed convective burning rates at $a_g = 0.001$ (Ri = 0.034). Thus, the burning rates for mixed convective burning approach the forced convective burning limit as a_g is decreased.

Aspect Ratio

As mentioned earlier in the section dealing with forced convective burning, the results for the total fuel burning rate (cylinder) approach the results of a flat plate as the radius is increased, keeping height fixed. To determine at what point increasing the radius would no longer affect the burning rate, the ratio of the total burning rates (cylinders of different aspect ratios compared to the flat plate solution) are plotted versus aspect ratio in Figure 4-21. The aspect ratio is defined as the wick height divided by the radius, H/y_o. As the aspect ratio is decreased (increasing radius), the total burning rate approaches the value of the flat plate solution. In the case of forced convective burning, an aspect ratio of less than 0.125 means the total burning rates for cylindrical and planar wicks differ by 1%. For mixed convective burning, the total fuel burning rates for cylindrical and planar wicks differ by 1% for an aspect ratio of 0.25. Figure 4-22 shows the local fuel burning rates for cylindrical wicks of radius 12.5, 50.8, and 100 mm, as well as the corresponding flat plate solution ($y_o \rightarrow \infty$). The curve for $y_o = 12.5$ mm deviates significantly from the flat plate solution; however, the curves for the other two cylindrical cases deviate only slightly from the flat plate solution. These results are similar to those found by Lyu and Chen (1991) for ethanol-air wick diffusion flames.

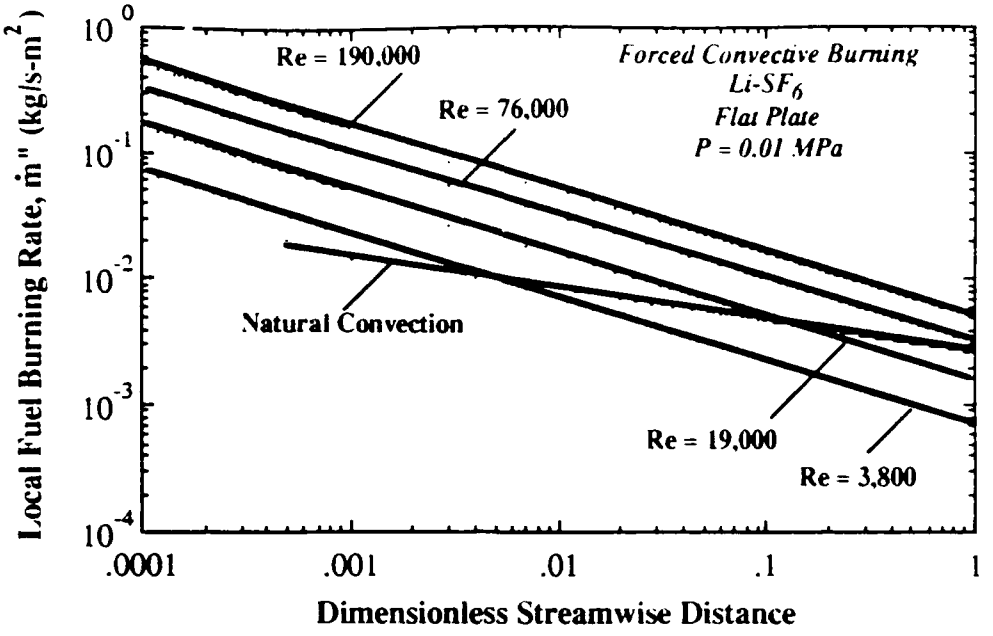

Figure 4-1. Predicted local fuel burning rates of planar Li-SF_6 wick diffusion flame; H = 100 mm.

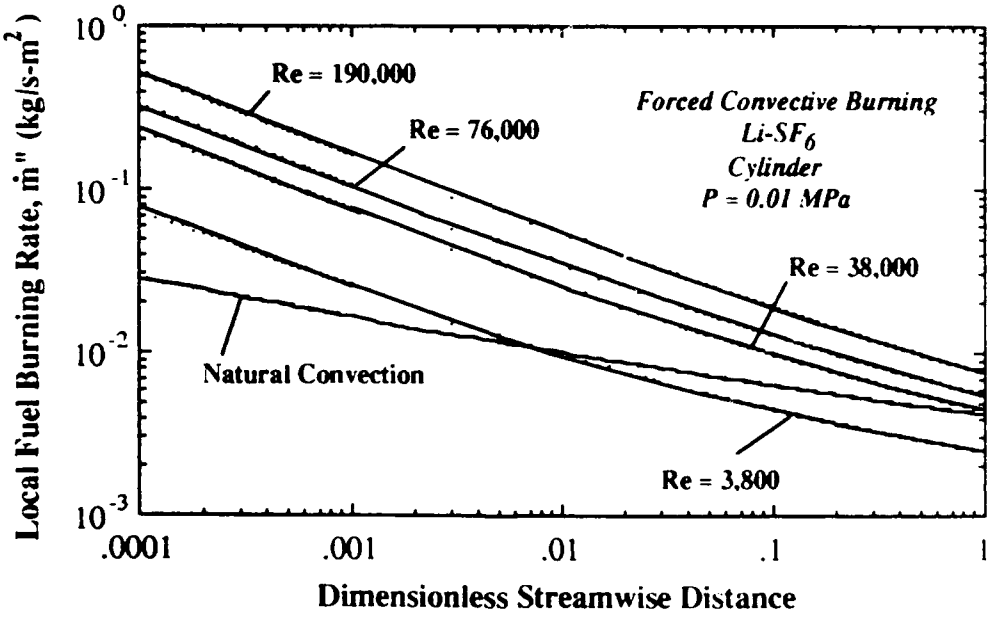

Figure 4-2. Predicted fuel burning rates of cylinder Li-SF_6 wick diffusion flame; H = 100 mm, y_o = 12.5 mm.

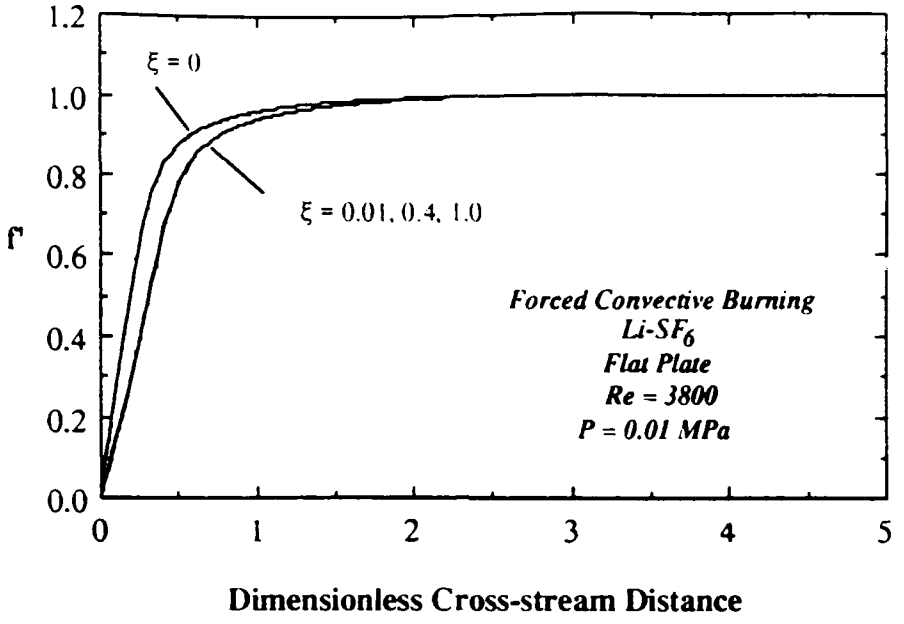

Figure 4-3. Similarity profiles of dimensionless streamwise velocity for wick-type Li-SF_6 diffusion flame; H = 100 mm, u_∞ = 1 m/s.

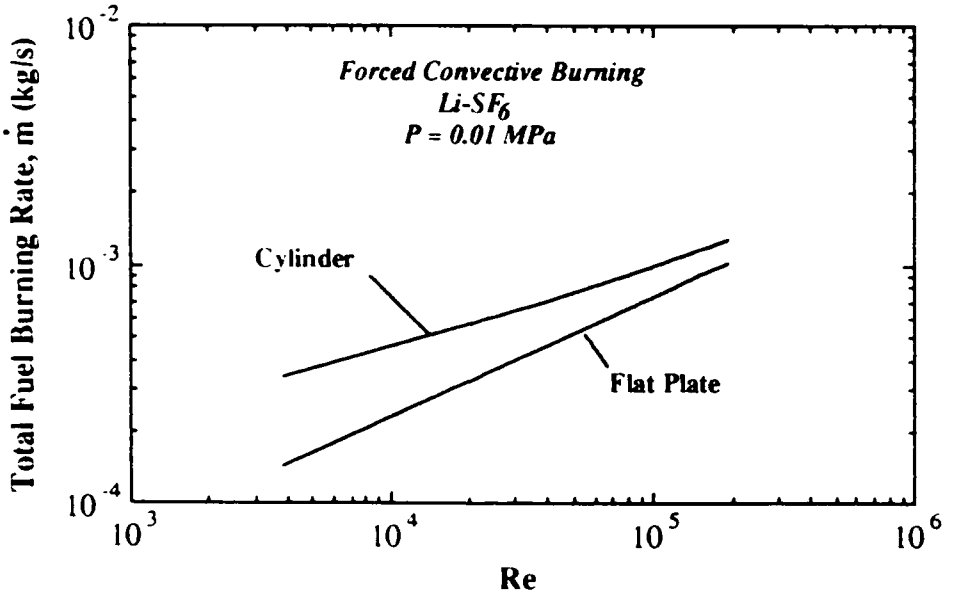

Figure 4-4. Predicted total fuel burning rates of flat-plate (H = 100 mm) and cylinder (H = 100 mm, y_o = 12.5 mm) Li-SF_6 wick diffusion flame as functions of Re.

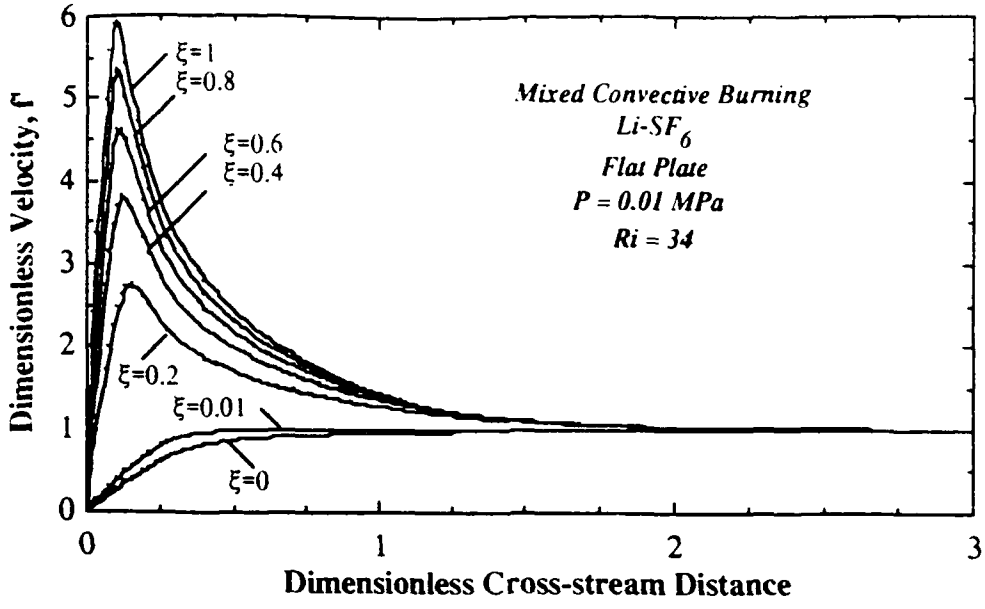

Figure 4-5. Dimensionless streamwise velocity of flat-plate Li-SF_6 wick diffusion flame; Ri = 34 (u_∞ = 1 m/s), H = 100 mm, a_g = 1.

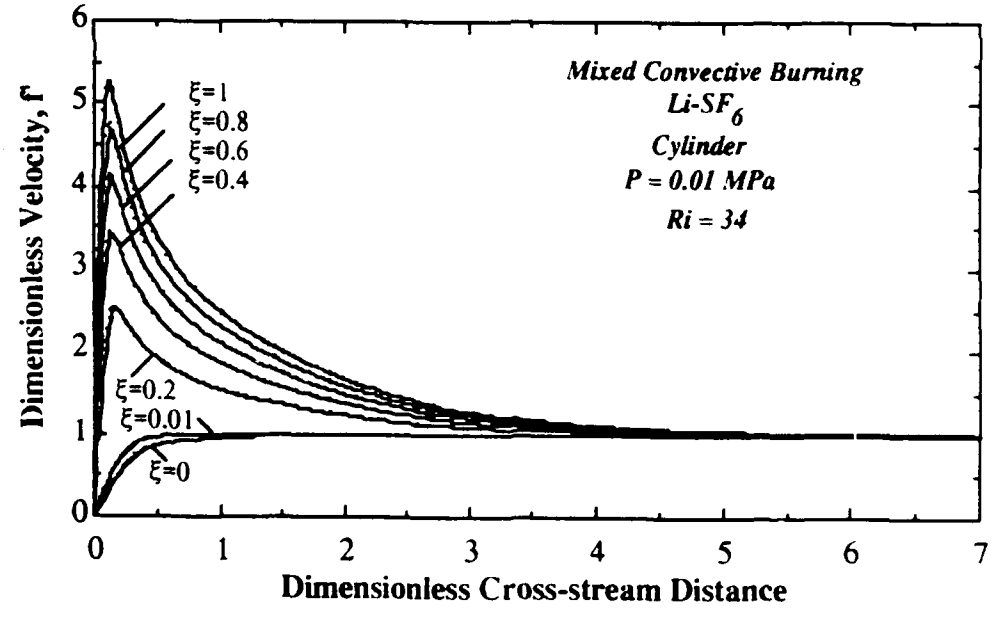

Figure 4-6. Dimensionless streamwise velocity of cylinder Li-SF_6 wick diffusion flame; Ri = 34 (u_∞ = 1 m/s), H = 100 mm, y_o = 12.5 mm, a_g = 1.

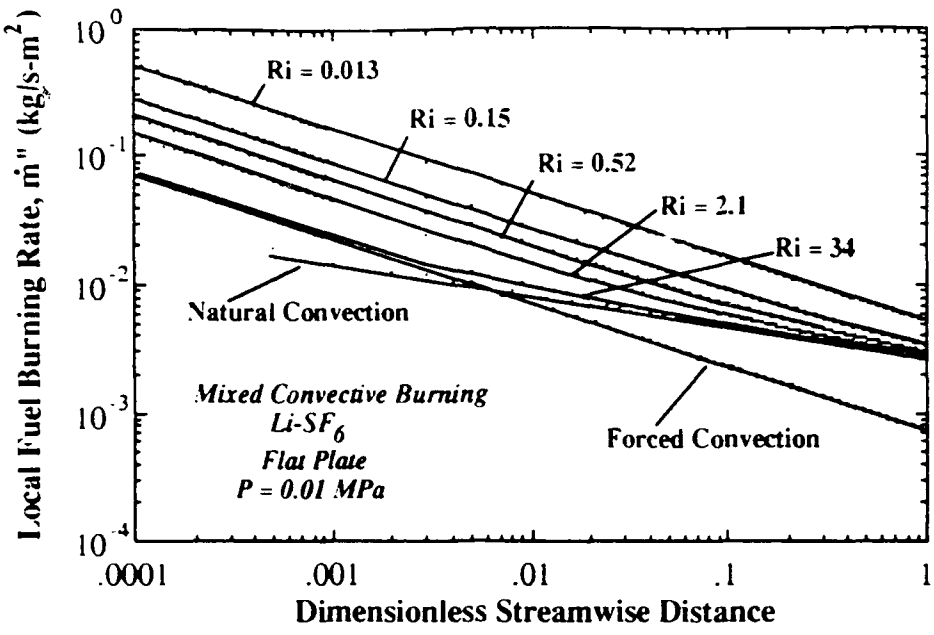

Figure 4-7. Predicted local fuel burning rates for flat-plate Li-SF_6 wick diffusion flame; H = 100 mm, a_g = 1.0, Gr = 4.93 x 10^8.

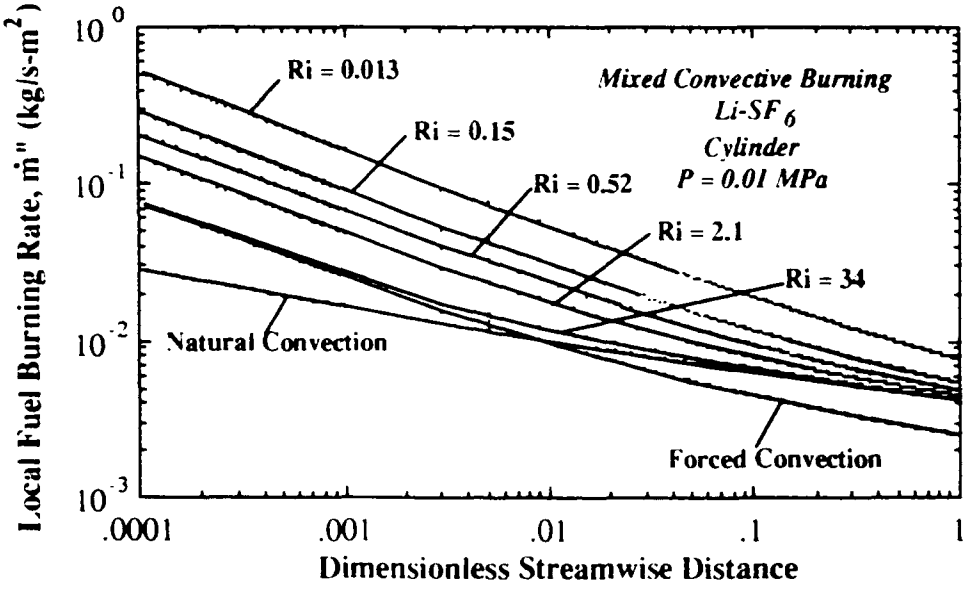

Figure 4-8. Predicted local fuel burning rates for cylindrical Li-SF_6 wick diffusion flame; H = 100 mm, a_g = 1.0, Gr = 4.93 x 10^8.

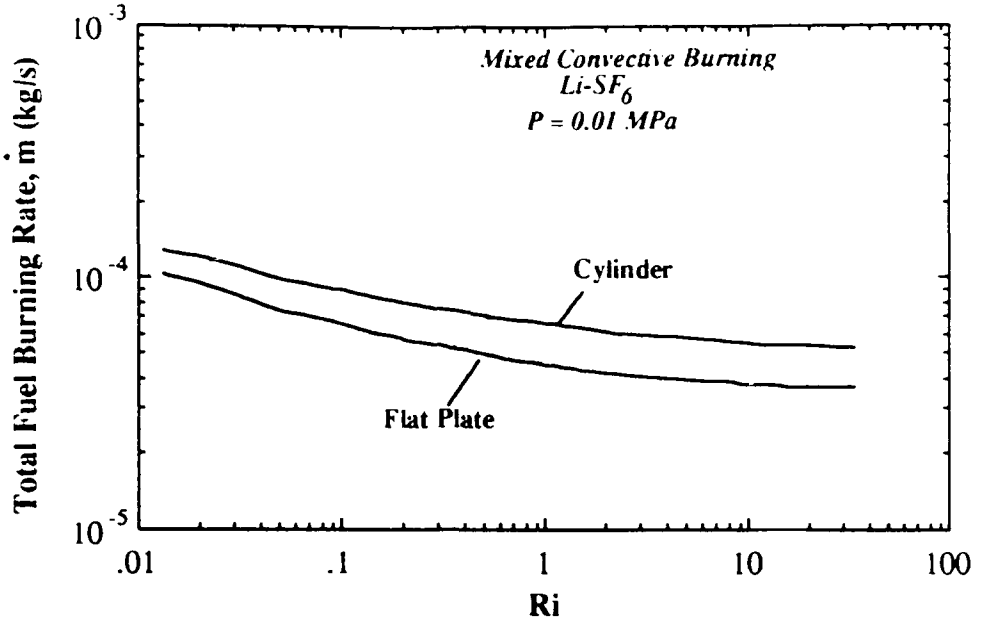

Figure 4-9. Predicted total fuel burning rates for flat-plate (H = 100 mm) and cylinder (H = 100 mm, y_o = 12.5 mm) Li-SF_6 wick diffusion flame as functions of Ri; a_g = 1.0, Gr = 4.93 x 10^8.

Table 4-1. Comparison of total fuel burning rates (kg/s) for cylinder (H = 100 mm, y_o = 12.5 mm).

Ri	$\dot{m}_{nc}$	$\dot{m}_{fc}$	$\dot{m}_{nc} + \dot{m}_{fc}$	$\dot{m}_{mc}$	% Difference
34	0.00035	0.00014	0.00049	0.00037	32
2.1	0.00035	0.00029	0.00064	0.00042	52
0.36	0.00035	0.00045	0.00080	0.00052	54
0.037	0.00035	0.00079	0.0011	0.00081	36
0.013	0.00035	0.0010	0.0014	0.0010	40

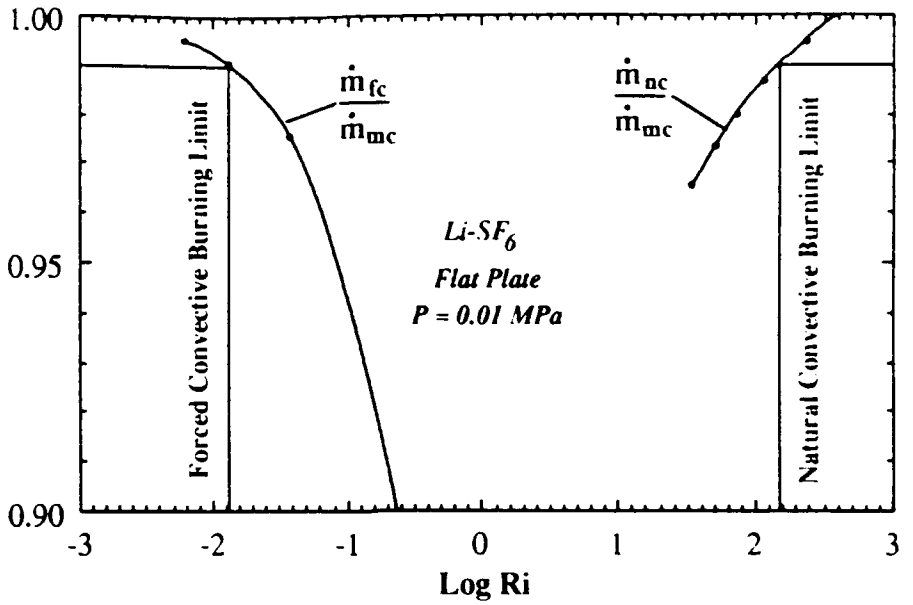

Figure 4-10. Critical Richardson numbers for natural and forced convective burning limits (99% accuracy); flat-plate Li-SF_6 wick diffusion flame; H = 100 mm, a_g = 1.0. $Ri_{cr,fc}$ = 0.013 and $Ri_{cr,nc}$ = 155.

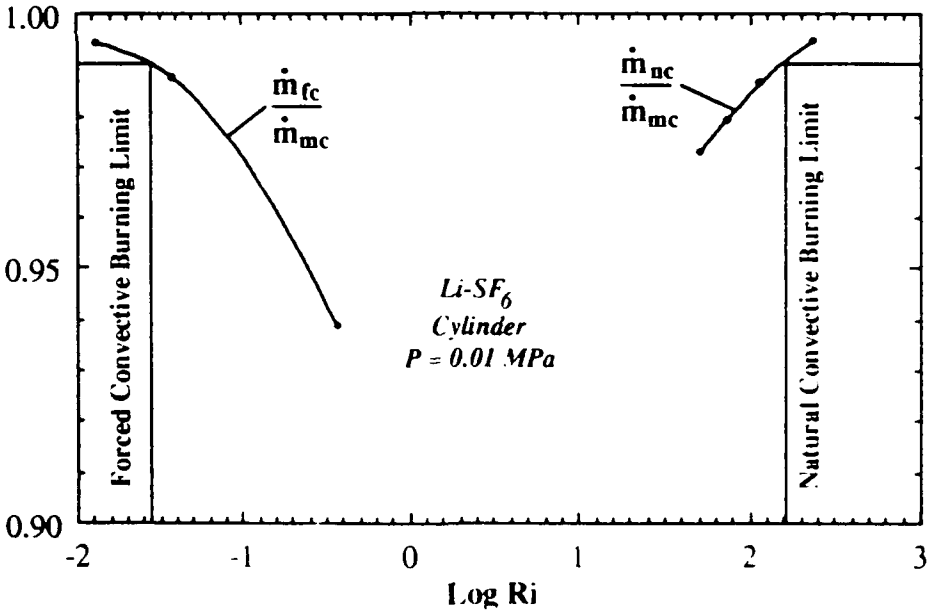

Figure 4-11. Critical Richardson numbers for natural and forced convective burning limits (99% accuracy); cylindrical Li-SF_6 wick diffusion flame; H = 100 mm, y_o = 12.5 mm, a_g = 1.0. $Ri_{cr,fc}$ = 0.028 and $Ri_{cr,nc}$ = 160.

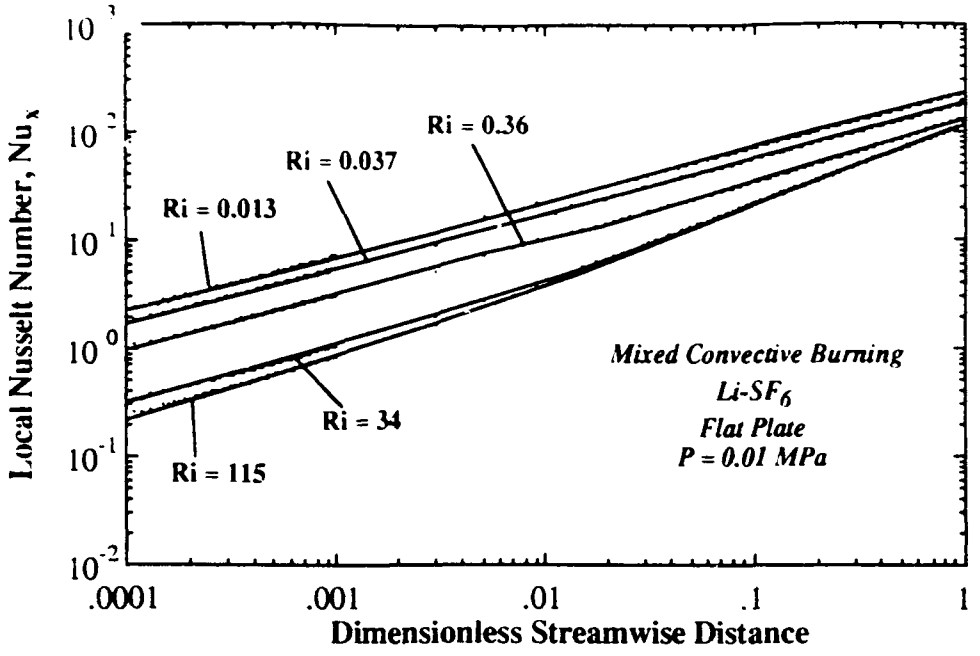

Figure 4-12. Predicted local Nusselt number for flat-plate Li-SF_6 wick diffusion flame; H = 100 mm, a_g = 1.0.

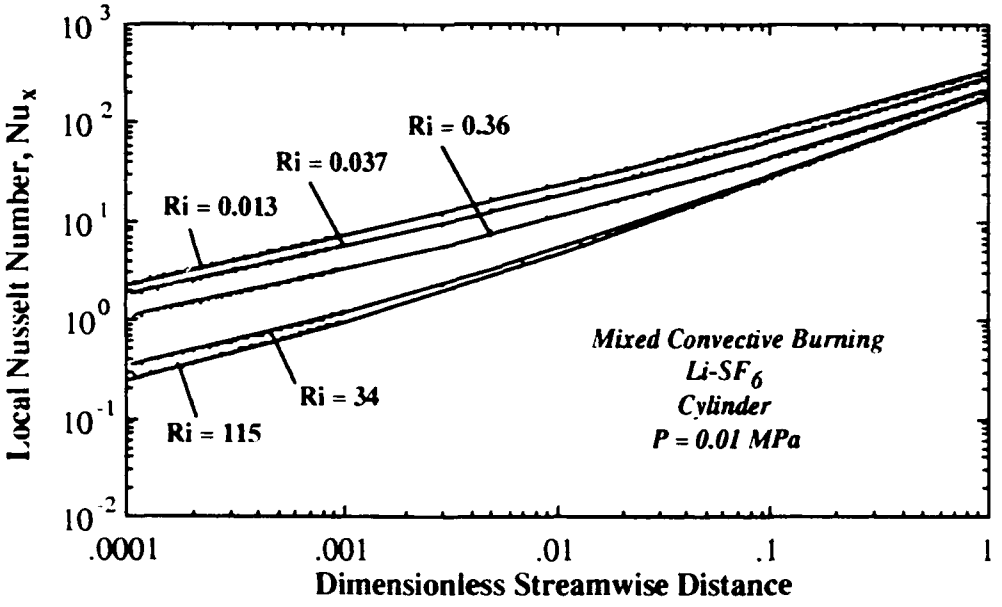

Figure 4-13. Predicted local Nusselt number for cylinder Li-SF_6 wick diffusion flame; H = 100 mm, y_o = 12.5 mm, a_g = 1.0.

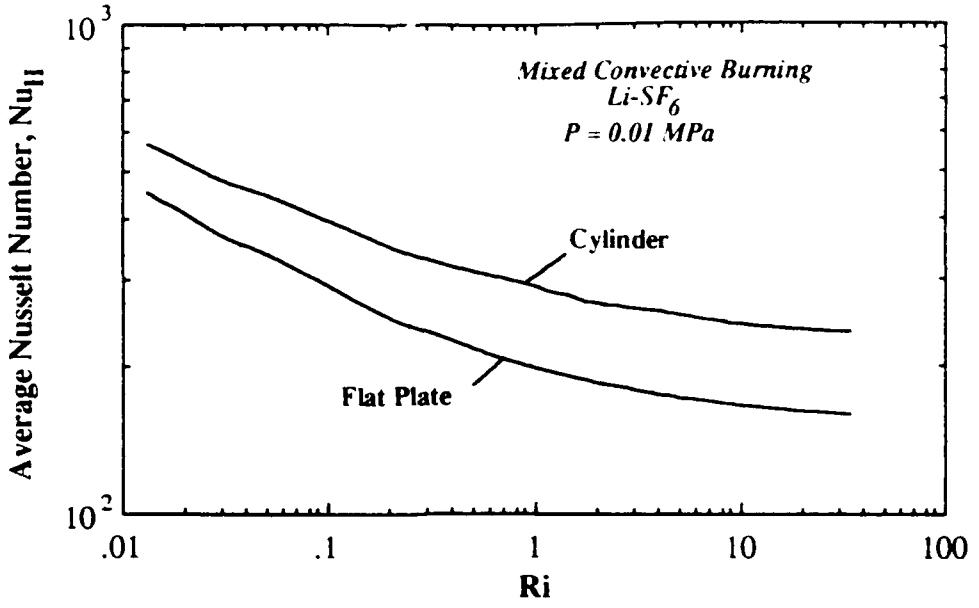

Figure 4-14. Predicted average Nusselt numbers for flat-plate (H = 100 mm) and cylinder (H = 100 mm, y_o = 12.5 mm) Li-SF_6 wick diffusion flame as functions of Ri; a_g = 1.0, Gr = 4.93 x 10^8.

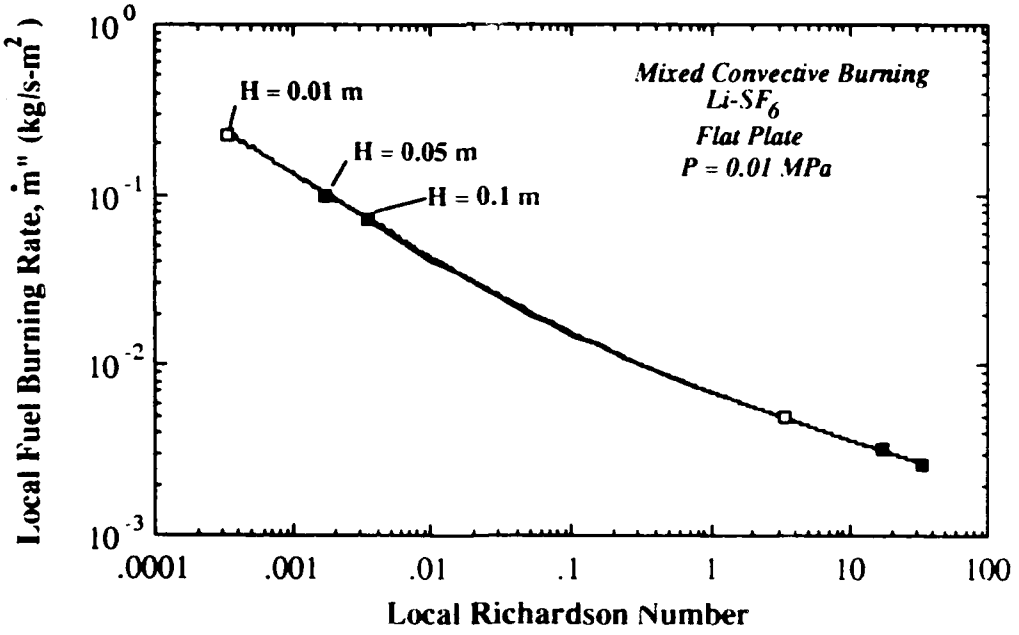

Figure 4-15. Effect of varying wick height on local fuel burning rate for planar wick (H = 0.1, 0.05, 0.01); u_∞ = 1 m/s, a_g = 1.

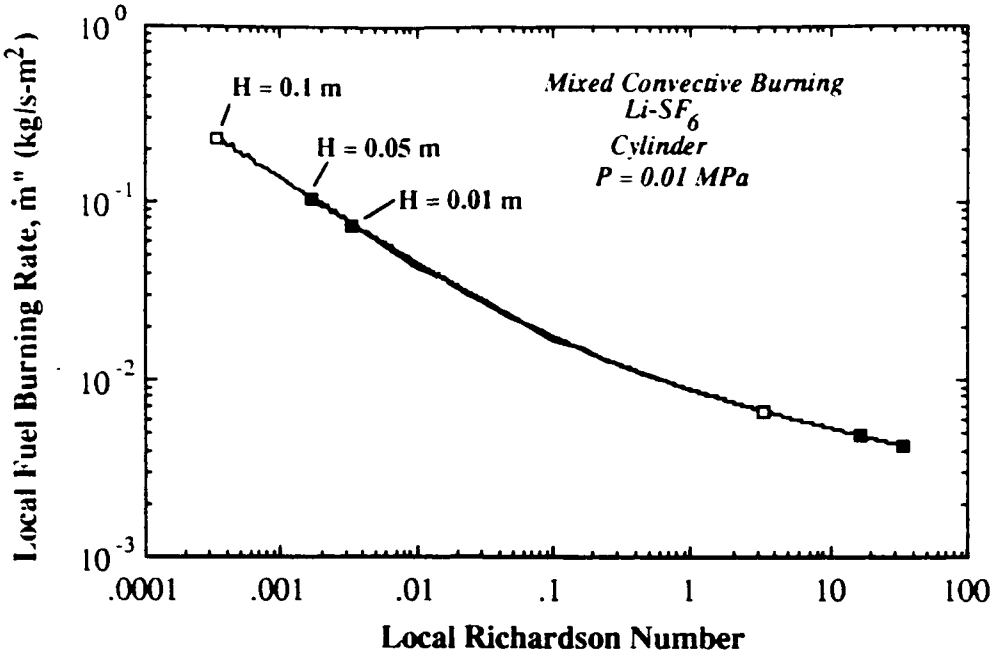

Figure 4-16. Effect of varying wick height on local fuel burning rate for cylindrical wick (H = 0.1, 0.05, 0.01); y_o = 12.5 mm, u_∞ = 1 m/s, a_g = 1.

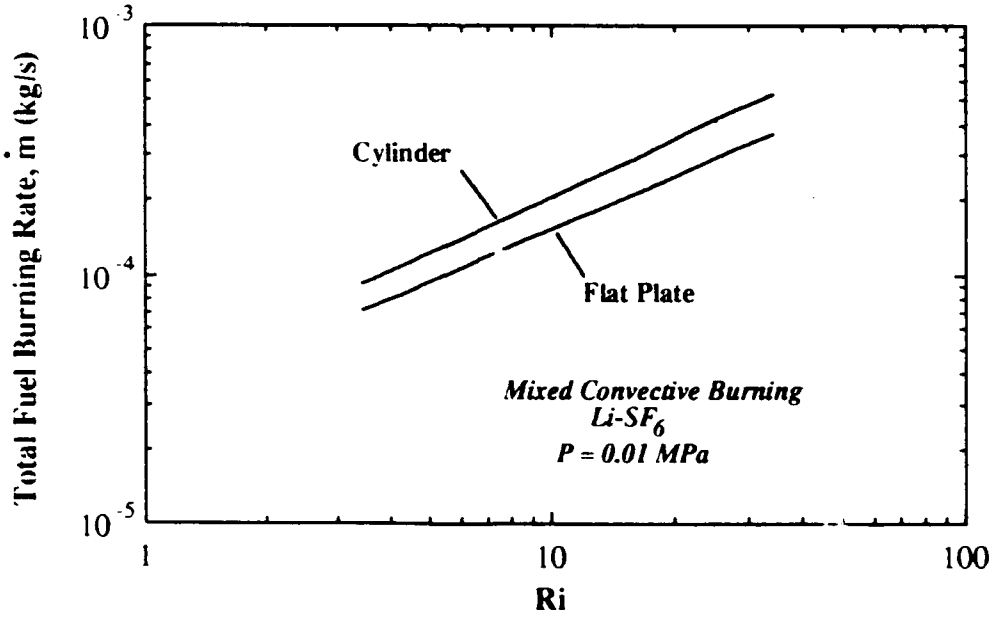

Figure 4-17. Predicted total fuel burning rate of Li-SF_6 wick combustion as function of Ri (H = 0.1, 0.075, 0.05, 0.025, 0.01 m); y_o = 12.5 mm, u_∞ = 1m/s, a_g = 1.0.

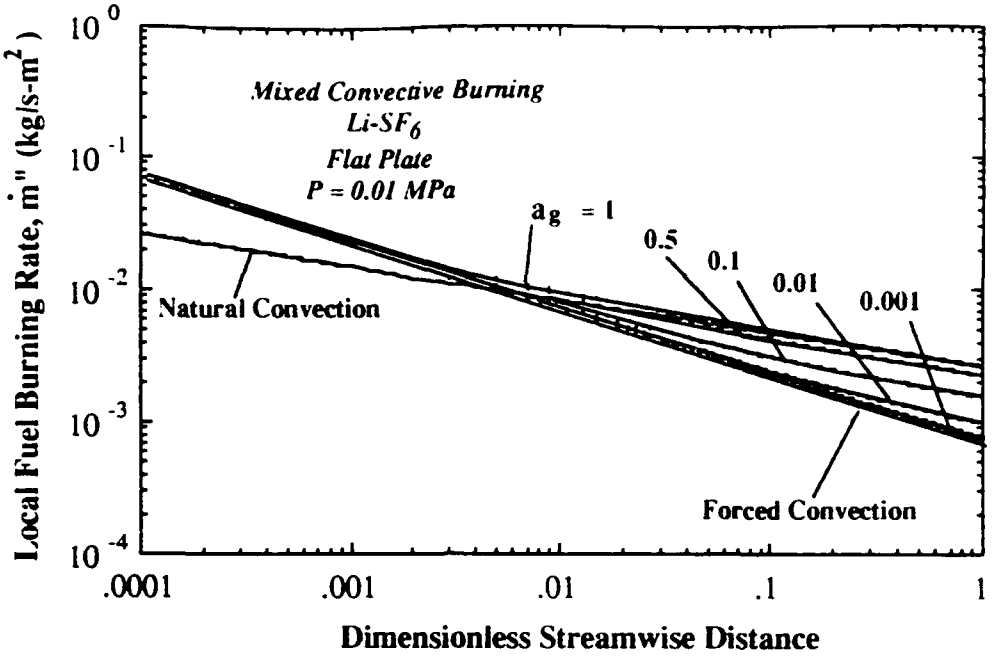

Figure 4-18. Effect of varying arbitrary gravitational constant, a_g, on local fuel burning rate for planar wick (a_g = 1, 0.5, 0.1, 0.01, 0.001); H = 100 mm, u_∞ = 1 m/s.

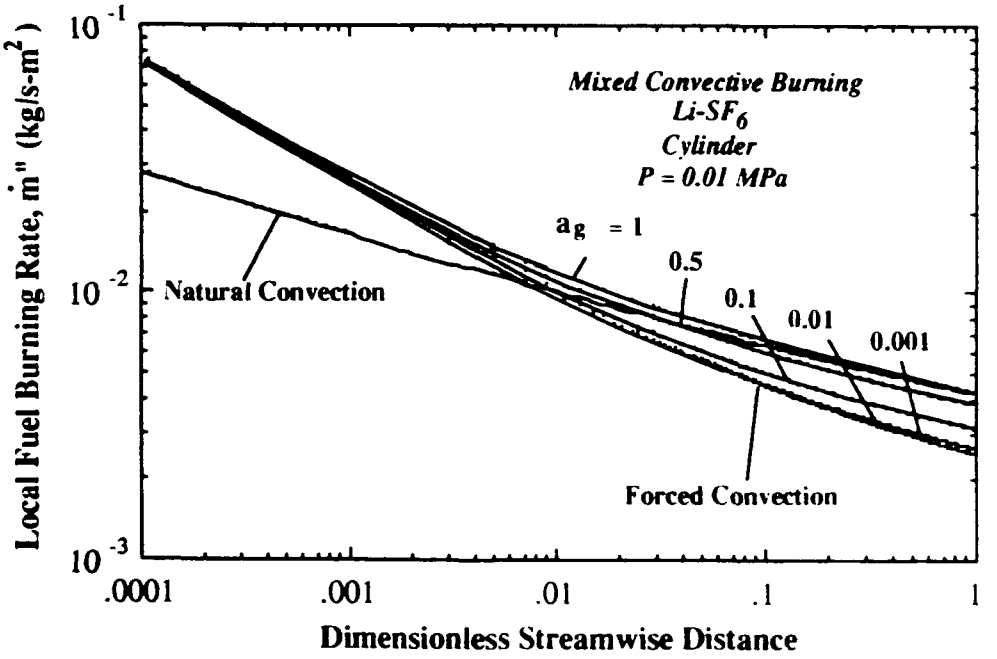

Figure 4-19. Effect of varying arbitrary gravitational constant, a_g, on local fuel burning rate for cylindrical wick (a_g = 1, 0.5, 0.1, 0.01, 0.001); H = 100 mm, y_o = 12.5 mm, u_∞ = 1 m/s.

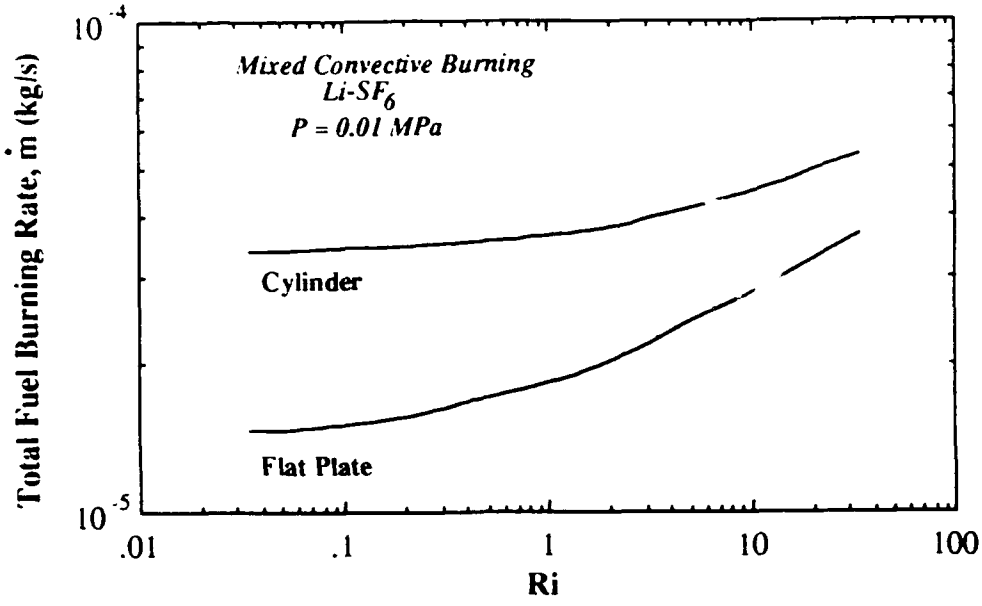

Figure 4-20. Predicted total fuel burning rates of planar and cylinder Li-SF_6 wick diffusion flames as function of Ri (a_g = 1, 0.5, 0.1, 0.01, 0.001); H = 100 mm, y_o = 12.5 mm, u_∞ = 1m/s.

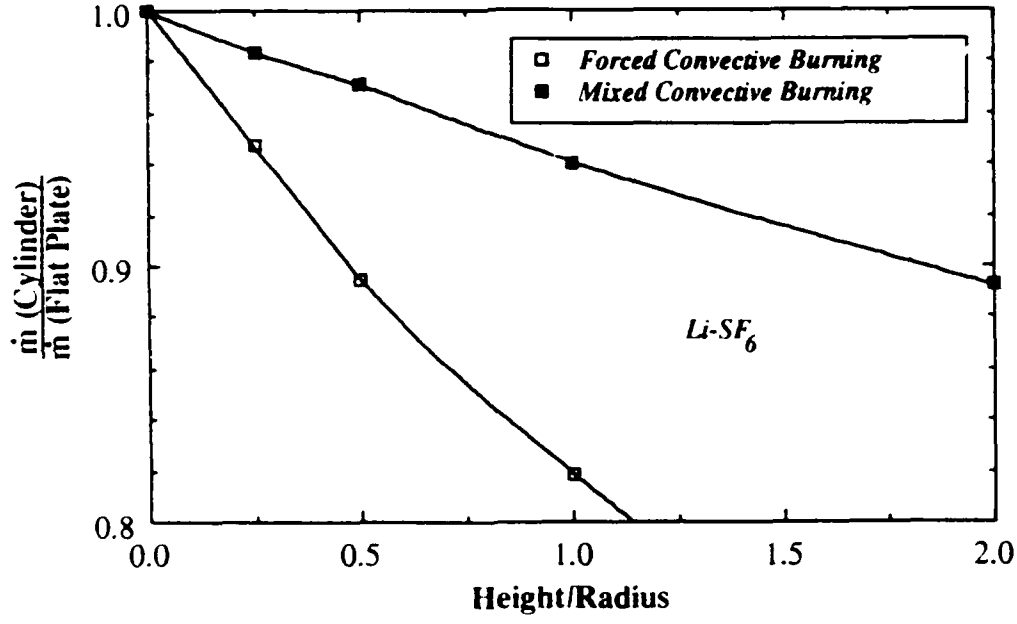

Figure 4-21. Ratio of total fuel burning rates (cylinder to flat plate) versus (H/y_o); variable radius, u_∞ = 1 m/s, H= 100 mm, a_g = 1; forced and mixed convective burning of Li-SF_6 wick diffusion flames.

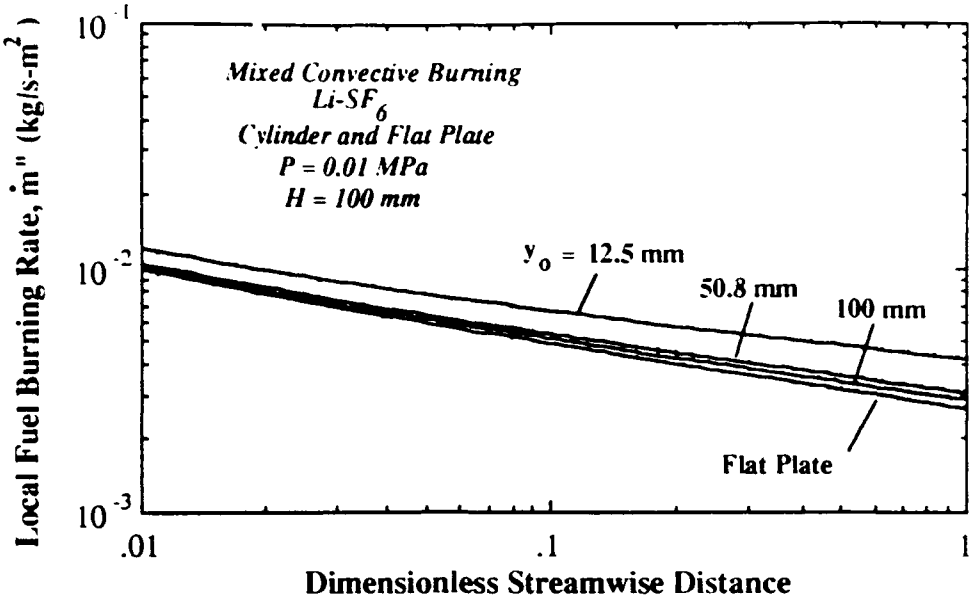

Figure 4-22. Predicted local fuel burning rates for flat-plate and cylinder (y_o = 12.5, 50.8, 100 mm) Li-SF_6 wick diffusion flames; u_∞ = 1 m/s, H = 100 mm, ag = 1.0.

CHAPTER 5

SUMMARY AND CONCLUSIONS

The objective of this study is to extend the methodology (developed for Li-SF_6 wick diffusion flames under natural convective burning conditions) to investigate forced and mixed convective burning of Li-SF_6 wick diffusion flames. A conserved scalar approach is employed to model the wick diffusion flames, and the interface condition is determined by the conservation of mass, species, and energy at the interface. Computation is first done for forced convective burning of Li-SF_6 wick diffusion flames and then extended to mixed convective burning. A limitation of the present analysis comes from the employment of boundary-layer approximations. The analysis, in essence, considers a semi-infinitely long wick. The end effects of a finite height wick are not considered.

In the process of obtaining numerical results, the computer code from Lyu (1991) was modified to calculate the local fuel burning rate. The code utilized the state relationships based on the converged interface condition (P = 0.01 MPa, Y_{Fw} = 0.38), which were already calculated by Lyu (1991), using the NASA CEC equilibrium code (Gordon and McBride, 1976). The computer program used a finite-difference scheme and marching procedure to solve the transformed governing equations. The numerical grid employed 600 points in the ξ-direction and 82 points in the η-direction. The total fuel burning rates were calculated using Simpson's rule of numerical integration over the length of the wick surface (from ξ_{min} = 0.0001 to ξ = 1).

Flow calculations involving forced convective burning were performed for both planar and cylindrical wick geometries. Similarity solutions were obtained for flat-plate

Li-SF_6 wick diffusion flames, i.e., $\dot{m}'' \propto \xi^{-1/2}$. Because of curvature effects, however, nonsimilar solutions were obtained for cylinder Li-SF_6 wick diffusion flames. In general, cylindrical wicks enhanced the burning such that the total fuel burning rates were higher. Flow calculations were then done for mixed convective burning. The results for the local fuel burning rates showed that forced convection dominates near the leading edge and natural convection over the rest of the surface The results indicated that natural convection has a large contribution to mixed convective burning.

A parametric study is done on the effects of varying the free-stream velocity (u_∞), the wick height (H), and the gravity (a_g) on the fuel burning rate. The starting values for each parameter were 1 m/s for u_∞, 100 mm for H, and 1.0 for a_g. Each calculation was done for both planar and cylindrical wick geometries. The effect of increasing u_∞ was to increase the local fuel burning rates. For the planar case, as u_∞ was increased, the burning curves were observed to have forced convective burning characteristics, i.e., $\dot{m}'' \propto \xi^{-1/2}$. Upon further investigation, critical Richardson numbers were found for a given geometry and gravity condition (H = 100 mm, y_0 = 12.5 mm, and a_g = 1.0); these numbers indicate when mixed convective burning can be approximated by either forced and natural convective burning. When the wick height H was decreased from 100 mm to 10 mm, the total burning rates were observed to decrease. A relationship between the total fuel burning rates and log Ri was obtained for both flat plates and cylinders. The local burning curves for different heights overlap one another when the burning rate is plotted versus the local Richardson number. When the gravity was decreased from 1.0 to 0.001, burning rates also decreased. The values of the local fuel burning rates near the leading edge, where forced convective burning dominates, remained relatively unaffected; however, downstream, where natural convection dominates, the local burning rates decreased noticeably due to the lower gravity, which resulted in smaller buoyancy forces. As a_g was decreased, the burning rates approached the forced convective burning

limit. Regarding the aspect ratio, the fuel burning rates for cylindrical wicks (both forced and mixed convective burning) approached the results for planar geometry. In the case of mixed convective burning, the local fuel burning rate for a cylindrical wick of height 100 mm and radius 50.8 mm deviated only slightly from the flat plate solution.

This study, though not a comprehensive treatment of mixed convective burning of Li-SF_6 wick diffusion flames, has accomplished its objectives. For one, a mathematical model was developed for wick-type Li-SF_6 diffusion flames undergoing mixed convective burning. Secondly, numerical solutions were obtained to assess the effects due to geometry (cylindrical versus planar wicks, varying wick heights and aspect ratios) and ambient conditions (free-stream velocity of oxidant, gravity) on the wick combustion of Li and SF_6. Thirdly, results were presented that will add to the knowledge base of earth-bound combustion experiments performed for variable gravity conditions. These results include establishing a relationship between the burning rate and the free-stream velocity, investigating the effects of reduced gravity on the wick combustion, and performing a sample calculation to determine the number of wicks needed to meet a heat output requirement.

Further analysis and experimentation are needed to evaluate the uncertainties of the analysis, as well as confirm the results predicted. Suggested future work includes extending the analysis to turbulent flow, incorporating radiative heat transfer into the analysis, analyzing the end effects of a finite wick, and considering the effects of the presence of non-condensable gases, such as argon.

REFERENCES

Cebeci, T. and Bradshaw, P., *Momentum Transfer in Boundary Layers*, McGraw-Hill, New York, 1977.

Chen, L.-D. and Faeth, G. M., "Ignition of Gases During Flow Near a Heated Surface," *Proceedings of the First International Specialty Meeting of the Combustion Institute*, Vol. 2, pp. 395-400, The Combustion Institute, 1981.

Chen, L.-D., Hsu, K.-Y., and Lyu, H.-Y., "Wick-Type Liquid-Metal Combustion," To Appear in *Proceedings of 3rd ONR Propulsion Meeting*, Newport, Rhode Island, October 15-17, 1990, Naval Underwater System Command, 1990.

Chen, L.-D., Hsu, K.-Y., and Lyu, H.-Y., "Wick-Type Liquid-Metal Combustion," Final Report to the Office of Naval Research (Grant No. 00014-89-J-1188; October 15, 1988 to April 14, 1991), The University of Iowa, 1991.

Damaso, R. C., "Mixed Convective Burning of Li-SF_6 Wick Diffusion Flames," M. S. Thesis, Department of Mechanical Engineering, The University of Iowa, 1992.

Damaso, R. C. and Chen, L.-D., "Forced Convective Burning of Li-SF_6 Wick Combustion," *AIAA/ASME/SAE/ASEE 28th Joint Propulsion Conference*, AIAA Paper No. 92-3379, 1992.

Gordon, S. and McBride, B. J., "Computer Program for Calculation of Complex Chemical Equilibrium," NASA SP-273, NASA, with the 1986 Version of the Transport Properties, 1976.

Groff, E. G., "Characteristics of a Steadily Operating Metal Combustor," Ph. D. Dissertation, Department of Mechanical Engineering, Pennsylvania State University, 1976.

Groff, E. G., and Faeth, G. M., "Steady Metal Combustor as a Closed Thermal Energy Source," *J. Hydronautics*, Vol. 12, No. 2, pp. 63-70, 1978.

Hsu, K.-Y., "An Experimental Study of Wick-Type Liquid-Metal Combustion," Ph.D. Dissertation, Department of Mechanical Engineering, The University of Iowa, Iowa City, Iowa, May 1991.

Hsu, K.-Y. and Chen, L.-D., "An Experimental Study of Li-SF6 Wick Combustion and Morphology Analysis of Combustion Products," AIAA Paper No. 91-2447, 1991.

Hsu, K.-Y. and Chen, L.-D., "Simultaneous Two-Line Optical Pyrometry for Lithium Combustion Measurements," AIAA Paper No. 92-0586, 1992.

Hughes, T. G., Smith, R. B., and Kiely, D. H., "Stored Chemical Energy Propulsion System for Underwater Applications," *AIAA J. Energy*, Vol. 7, pp. 128-133, 1983.

Jaluria, Y., "Mixed Convection Flow over Localized Multiple Thermal Sources on a Vertical Surface," *Physics of Fluids*, Vol. 29, No. 4, pp. 934-940, 1986

Jaluria, Y. and Tewari, S. S., "Mixed Convection Heat Transfer From Thermal Sources Mounted on Horizontal and Vertical Surfaces," *Journal of Heat Transfer*, Vol. 112, pp. 975-987, 1985.

Lyu, H.-Y., "Modeling of Liquid-Metal Wick Diffusion Flames," Ph.D. Dissertation, Department of Mechanical Engineering, The University of Iowa, Iowa City, Iowa, May 1991.

Lyu, H.-Y. and Chen, L.-D., "Ethanol-Air Wick Diffusion Flames," in *ASME-JSME Thermal Engineering - 1991*, Vol. 5, pp. 311-317, ASME, 1991 (a).

Lyu, H.-Y. and Chen, L.-D., "Numerical Modeling of Buoyant Ethanol-Air Wick Diffusion Flames," *Combustion and Flame*, Vol. 87, pp. 169-181, 1991 (b).

Lyu, H.-Y., Chen, L.-D. and Hsu, K.-Y., "Wick-Type Liquid-Metal Combustion," *AIAA J. Propulsion and Power* (in press); Also as AIAA Paper No. 90-2477, 1990.

Weltner, K., Grosjean, J., Schuster, P., Weber, W. J., *Mathematics for Engineers and Scientists*, Stanley Thornes, Chltenham, England, pp. 413-422, 1986.

Williams, F. A., *Combustion Theory*, 2nd Ed., Benjamin/Cummings, Menlo Park, California, pp. 1-18, 1985.

Wu, S. H. and Chen, L.-D., "Direct Numerical Simulation of Unsteady Wick Diffusion Flame," *AIAA Journal of Propulsion and Power*, Vol. 8, 1992 (in press).

Yao, L.-S., "Two-Dimensional Mixed Convective Burning Along a Flat Plate," *Proceedings Winter Annual Meeting of ASME, Heat Transfer Division*, Vol. 53, pp. 33-38, 1985.

APPENDIX A

COMPUTER PROGRAM FOR FLOW CALCULATION

Main Program

```
C*************************************************************************
C FILENAME: FLOW.MC.C.V.U1          (U__ DENOTES FREE-STREAM VELOCITY)
C COMMENTS: THIS IS THE FLOW CALCULATION PROGRAM FOR MIXED CONVECTION
C * CYLINDER: CURVAT NOT EQUAL TO 0      DIMENSIONS: H=0.1 M AND R=12.5 MM
C * VARIABLE PROPERTIES: LI AND SF6      SYSTEM PRESSURE = 0.1 MPA
C * YFW = 0.38 (CONVERGED INTERFACE CONDITION)
C * OUTPUT: LOCAL FUEL BURNING RATE RMBR
C*************************************************************************
      IMPLICIT REAL*8(A-H,O-Z),INTEGER*4(I-N)
      COMMON /INPT1/ A1,A2,A1Z,ALFA0,ALFA1,IT,IFLAG,GR,RJA,
     1       HPLATE,RADIUS,RKVISI,RE,UINF,RI
      COMMON /EOS2/ ZMF(101),RHO(101),TEP(101),RHOM(200),TEMP(200),
     1       DVC(101),PR(101),DVCM(200),PRM(200),JC
      COMMON /ETA3/ ETAE,NP6,NP,DETA(200),ETA(200),A(200),NPC,NNP,NXT,
     1       NX,X(600),CVW,VW(2),VWT
      COMMON /REST4/ F(200,2),U(200,2),V(200,2),Z(200,2),P(200,2),
     1       AM(200,2),B(200,2),BZ(200,2),BT(200)
      COMMON /SOLV6/ DELF(200),DELU(200),DELV(200),DELZ(200),
     1       DELP(200),ABSERR
C=========================================================================
      ITMAX = 900
      NX = 1
C-------------------------------------------------------------------------------------------------------------
C     SUBROUTINE INPUT SUPPLIES FLOW GEOMETRY AND PROPERTY CONSTANTS
C     A1,A2:          MOMENTUM EQUATION PARAMETERS
C     A1Z:            MIXTURE FRACTION PARAMETERS
C     ALFA0,ALFA1:    BOUNDARY CONDITIONS PARAMETER
C     IFLAG:          CONTROL PARAMETER
C     GR:             GRASHOF NUMBER
C     HPLATE:         LONGITUDINAL LENGTH
C     RADIUS:         RADIUS OF CYLINDER
C     RKVISI:         KINEMATIC VISCOSITY AT INFINITY
C     RJA:            MODIFIED JACOB NUMBER
C     RE:             REYNOLDS NUMBER
C     UINF:           VELOCITY AT INFINITY
C     RI:             RICHARDSON NUMBER (GR/RE^2)
C-----------------------------------------------------------------
      CALL INPUT
C-----------------------------------------------------------------
C     SUBROUTINE GRID SET UP GRID SYSTEM
C     NXT:            TOTAL GRID POINT IN X-DIRECTION
```

```
C       X(NX):          GRID POSITION IN X-DIRECTION
C       ETAE:           BOUNDARY LAYER THICKNESS
C       ETA(J):         GRID POSITION IN Y-DIRECTION
C       DETA(J):        INCREMENT OF GRID POSITION IN Y-DIRECTION
C       VGP:            RATIO OF ADJACENT GRIDS IN Y-DIRECTION
C       NP:             TOTAL GRID POINT IN Y-DIRECTION
C-----------------------------------------------------------------------------------------------------------
        CALL GRID
C-----------------------------------------------------------------------------------------------------------
C       SUBROUTINE IVZPL PRODUCES INITIAL GUESS PROFILES AND BOUNDARY
C       CONDITIONS FOR FLOW CALCULATION
C       F(J,2):  DIMENSIONLESS STREAM FUNCTION
C       U(J,2):  DIMENSIONLESS STREAMWISE VELOCITY
C       V(J,2):  DERIVATIVE OF U(J)
C       Z(J,2):  MIXTURE FRACTION
C       P(J,2):  DERIVATIVE OF Z(J)
C-----------------------------------------------------------------------------------------------------------
        CALL IVZPL
        IFLAG = 1
10      IT = 0
20      IT = IT + 1
        IF( IT .LT. ITMAX ) THEN
C-----------------------------------------------------------------------------------------------------------
C       SUBROUTINE INUPD INITIALIZE AND UPDATE PARAMETERS AND CALCULATE
C       CURVATURE TERM
C       AM(J,2):        MOMENTUM SOURCE TERM
C       B(J,2):         PROPERTY TERM IN MOMENTUM EQUATION
C       BZ(J,2):        PROPERTY TERM IN MIXTURE FRACTION EQUATION
C-----------------------------------------------------------------------------------------------------------
        CALL INUPD
        CALL COEF
        CALL SOLV5
        IF( ABSERR .GT. 1.D-06) THEN
        GO TO 20
        ELSEIF( DABS( V(NP,2) ) .GT. 1.D-03 ) THEN
        CALL GROW TH
C       WRITE(6,1000) NNP
        1000    FORMAT(1H0, 'ETAE GROW ',I3,' -POINTS ADDED')
        GO TO 10
        ENDIF
        ELSE
C       WRITE(6,2000) NX,X(NX),DELV(1),DELP(1)
2000    FORMAT(1H0,4HNX =,I3,5X,3HX =,E10.4,5X,25HITERATIONS EXCEEDED
      1         ITMAX,5X,7HDELVW =,E10.4,5X,7HDELZW =,E10.4)
        ENDIF
C-----------------------------------------------------------------------------------------------------------
C       CORRECT WALL BLOWING VELOCITY ACCORDING TO ENERGY AND SPECIES
C       WALL BOUNDARY CONDITIONS
C-----------------------------------------------------------------------------------------------------------
        IF( NX .NE. 1) THEN
        VWT = VW(2)
C       VW(2) = -( P(1,2) + ZPWT )/2.D+00*( GR/X(NX) )**2.5D-01/RJA
        VW(2) =          -P(1,2) * (RE/X(NX))**5.0D-01/RJA
C       VW(2) = -( P(1,2) + ZPWT )/2.D+00*DSQRT( RE/X(NX) )/RJA
        ZPWT = P(1,2)
```

```
      IF( DABS( VW(2) - VWT ) .GT. 1.D-08 ) THEN
      F(1,2) = F(1,1)*( X(NX-1)/X(NX) )**5.0D-01
     1         + CVW*( VW(1) + VW(2) )/2.D+00*( X(NX) - X(NX - 1) )
     2         /X(NX)**5.0D-01
      GO TO 20
      ELSE
      VW(1) = VW(2)
      ENDIF
      ENDIF
      CALL OUTPUT
      IF( NX .LE. NXT ) THEN
      GO TO 10
      ENDIF
      WRITE(6,514)
514   FORMAT(1H0,'MAIN: PROGRAM HAS EXECUTED')
      STOP
      END
      SUBROUTINE INPUT
      IMPLICIT REAL*8(A-H,O-Z),INTEGER*4(I-N)
      COMMON /INPT1/ A1,A2,A1Z,ALFA0,ALFA1,IT,IFLAG,GR,RJA,
     1         HPLATE,RADIUS,RKVISI,RE,UINF,RI
      COMMON /EOS2/ ZMF(101),RHO(101),TEP(101),RHOM(200),TEMP(200),
     1         DVC(101),PR(101),DVCM(200),PRM(200),JC
C=============================================================================
      A1 = 1.D+00
      A2 = 0.D+00
      A1Z = 1.D+00
C-----------------------------------------------------------------------------
C     ALFA0 = 1, ALFA1 = 0   SPECIFY FUNCTION VALUE
C     ALFA0 = 0, ALFA1 = 1   SPECIFY FUNCTION DERIVATIVE
C-----------------------------------------------------------------------------
      ALFA0 = 1
      ALFA1 = 0
C-----------------------------------------------------------------------------
C     READ IN CONSERVED SCALAR, TEMPERATURE, DENSITY, VISCOSITY, AND
C     PRANDTL NUMBER FROM CEC72 CALCULATION (FROM BLOCK DATA AT END)
C      ** SUPPRESS PROPERTIES FOR BLASIUS SOLUTION **
C-----------------------------------------------------------------------------
      READ(5,1000) ( ZMF(J),TEP(J),RHO(J),DVC(J),PR(J),J = 1,101 )
1000  FORMAT(F7.4,5X,F7.1,5X,E11.4,5X,E11.4,5X,F6.4)
C     DO 20 J=1,101
C     RHO(J) = 5.9696D-01
C     DVC(J) = 1.5710D-05
C     PR(J)  = 0.7368D+00
C20   CONTINUE
C-----------------------------------------------------------------------------
C     FLOW AND GEOMETRY CONSTANTS
C     YFW:          FUEL MASS FRACTION AT WALL
C     CPW:          SPECIFIC HEAT AT WALL
C     RKMW:         THERMAL CONDUCTIVITY OF MIXTURE AT WALL
C     DYFDZ:        DERIVATIVE OF FUEL MASS FRACTION W.R.T. MIXTURE FRACTION
C-----------------------------------------------------------------------------
      HPLATE = 1.D-01
      RKVISI = 1.55725D-05/RHO(1)
      GR = 9.80665D+00*DABS( RHO(1)/RHO(101) - 1.D+00 )*HPLATE**3.D+00
```

```
     1          /RKVISI/RKVISI
           YFW = 3.84741D-01
           CPW = 2.7935D+03
           RKMW = 7.315D-02
           DYFDZ = 7.6273D-01
C          RJA = DSQRT( 2.D+00 )*HPLATE*( 1.D+00 - YFW )*RHO(1)*CPW/RKMW
           RJA = DSQRT( 2.D+00 )*HPLATE*( 1.D+00 - YFW )*RHO(1)*CPW/RKMW/DYFDZ
           RADIUS = 1.25D-02
           UINF=1.D+00
           RE=UINF*HPLATE/RKVISI
           RI=GR/RE/RE
           RETURN
           END
           SUBROUTINE GRID
           IMPLICIT REAL*8(A-H,O-Z),INTEGER*4(I-N)
           COMMON /ETA3/ ETAE,NP6,NP,DETA(200),ETA(200),A(200),NPC,NNP,NXT,
     1          NX,X(600),CVW,VW(2),VWT
C==========================================================================
           NXT = 600
           DXP = 2.D-03
           DXP0 = 1.0D-05
           L = 101
           DETA(1) = 1.D-02
           VGP = 1.05D+00
           ETAE = 1.0D+04
C----------------------------------------------------------------------
C          GRID GENERATION IN X-DIRECTION
C----------------------------------------------------------------------
           X(1) = 0.D+00
           DO 95 I=2,L
           X(I) = X(I-1) + DXP0
95         CONTINUE
           DO 100 I = L+1,NXT
           X(I) = X(I-1) + DXP
100        CONTINUE
C----------------------------------------------------------------------
C          GRID GENERATION IN Y-DIRECTION
C----------------------------------------------------------------------
           IF( (VGP -1.D+00) .GT. 1.D-03 ) THEN
           NP = DLOG( ETAE/DETA(1)*(VGP - 1.D+00) + 1.D+00 )
     1          /DLOG(VGP) + 1.0001D+00
           NP6 = DLOG( 6.D+00/DETA(1)*(VGP - 1.D+00) + 1.D+00 )
     1          /DLOG(VGP) + 1.0001D+00
           ELSE
           NP = ETAE/DETA(1) + 1.0001D+00
           ENDIF
           IF( NP .LE. 310 ) THEN
           ETA(1) = 0.D+00
           DO 200 J = 2,NP
           DETA(J) = VGP*DETA(J-1)
           A(J) = DETA(J-1)/2.D+00
           ETA(J) = ETA(J-1) + DETA(J)
200        CONTINUE
           ELSE
           WRITE(6,1000)
```

```
1000    FORMAT(1H0,'NP EXCEEDED MAXIMUM ARRAY DIMENSION ALLOWED      --
     1          PROGRAM TERMINATED')
        STOP
        ENDIF
        RETURN
        END
        SUBROUTINE IVZPL
        IMPLICIT REAL*8(A-H,O-Z),INTEGER*4(I-N)
        COMMON /INPT1/ A1,A2,A1Z,ALFA0,ALFA1,IT,IFLAG,GR,RJA,
     1          HPLATE,RADIUS,RKVISI,RE,UINF,RI
     1          NX,X(600),CVW,VW(2),VWT
        COMMON /REST4/ F(200,2),U(200,2),V(200,2),Z(200,2),P(200,2),
     1          AM(200,2),B(200,2),BZ(200,2),BT(200)
        COMMON /SOLV6/ DELF(200),DELU(200),DELV(200),DELZ(200),
     1          DELP(200),ABSERR
C=============================================================
        ETA6 = 6.D+00 + 5.D-01
C-------------------------------------------------------------
C       GENERATE INITIAL PROFILE BY SOLVING THE INCOMPRESSIBLE FLOW
C-------------------------------------------------------------
        DO 100 J = 1,NP6
        ETAR = ETA(J)/ETA6
        ETAR2 = ETAR*ETAR
        F(J,2) = ETA6/4.D+00*ETAR2*( 3.D+00 - ETAR2/2.D+00 )
        U(J,2) = ETAR*( 1.5D+00 - ETAR2/2.D+00 )
        V(J,2) = 1.5D+00*( 1.D+00 - ETAR2 )/ETA6
        Z(J,2) = 1.D+00 - ETAR
        P(J,2) = -1.D+00/ETA6
100     CONTINUE
C-------------------------------------------------------------
C       INITIAL VALUE OF BOUNDARY CONDITIONS
C-------------------------------------------------------------
        U(NP6,2) = 1.D+00
        Z(NP6,2) = 0.D+00
        VW(1) = 0.D+00
        VW(2) = 0.D+00
C-------------------------------------------------------------
C       GENERATE BETTER PROFILES
C       IFLAG = 0, ETAE = ETA6 = 6.D+00
C       IFLAG =1, ETAE = ETAE
C-------------------------------------------------------------
        IFLAG = 0
        IT = 0
10      IT = IT + 1
C-------------------------------------------------------------
C       INITIALIZE AND UPDATE PROFILES
C-------------------------------------------------------------
        CALL INUPD
        IF( IT .GT. 100) THEN
        WRITE(6,1000)
1000    FORMAT(1H0,'INCOMPRESSIBLE FLOW SOLUTION DID NOT CONVERGE')
        STOP
        ELSE
        CALL COEF
        CALL SOLV5
```

```
      IF( ABSERR .GT. 1.D-06 ) GO TO 10
      ENDIF
C-----------------------------------------------------------------------
C     SET UP DUMMY NODES
C-----------------------------------------------------------------------
      DO 200 J = NP6+1,NP
      F(J,2) = F(NP6,2)
      U(J,2) = U(NP6,2)
      V(J,2) = V(NP6,2)
      Z(J,2) = Z(NP6,2)
      P(J,2) = P(NP6,2)
200   CONTINUE
      RETURN
      END
      SUBROUTINE COEF
      IMPLICIT REAL*8(A-H,O-Z),INTEGER*4(I-N)
      COMMON /INPT1/ A1,A2,A1Z,ALFA0,ALFA1,IT,IFLAG,GR,RJA,
     1       HPLATE,RADIUS,RKVISI,RE,UINF,RI
      COMMON /ETA3/ ETAE,NP6,NP,DETA(200),ETA(200),A(200),NPC,NNP,NXT,
     1       NX,X(600),CVW,VW(2),VWT
      COMMON /REST4/ F(200,2),U(200,2),V(200,2),Z(200,2),P(200,2),
     1       AM(200,2),B(200,2),BZ(200,2),BT(200)
      COMMON /COEF5/ S1(200),S2(200),S3(200),S4(200),S5(200),S6(200),
     1       S7,S8,B1(200),B2(200),B3(200),B4(200),
     2       B5(200),B6(200),B7(200),B8(200),R(5,200)
      C=======================================================
      IF( IT .EQ. 1) THEN
      CEL = 0.D+00
      IF( NX .GT. 1) THEN
      CEL = 1.D+00*( X(NX) + X(NX - 1) )/( X(NX) - X(NX - 1) )
      ENDIF
      P1P = A1 + CEL
      P2P = A2 + CEL
      P1PZ = A1Z + CEL
      ENDIF
C-----------------------------------------------------------------------
C     PRESENT STATION
C-----------------------------------------------------------------------
      DO 100 J = 2,NPC
      FB = ( F(J,2) + F(J-1,2) )/2.D+00
      UB = ( U(J,2) + U(J-1,2) )/2.D+00
      VB = ( V(J,2) + V(J-1,2) )/2.D+00
      ZB = ( Z(J,2) + Z(J-1,2) )/2.D+00
      PB = ( P(J,2) + P(J-1,2) )/2.D+00
      AMB = ( AM(J,2) + AM(J-1,2) )/2.D+00
      FVB = ( F(J,2)*V(J,2) + F(J-1,2)*V(J-1,2) )/2.D+00
      USB = ( U(J,2)*U(J,2) + U(J-1,2)*U(J-1,2) )/2.D+00
      FPB = ( F(J,2)*P(J,2) + F(J-1,2)*P(J-1,2) )/2.D+00
      UZB = ( U(J,2)*Z(J,2) + U(J-1,2)*Z(J-1,2) )/2.D+00
      DBV = ( B(J,2)*V(J,2) - B(J-1,2)*V(J-1,2) )/DETA(J - 1)
      DBZP = ( BZ(J,2)*P(J,2) - BZ(J-1,2)*P(J-1,2) )/DETA(J - 1)
      IF( NX .EQ. 1) THEN
C-----------------------------------------------------------------------
C     PREVIOUS STATION
C-----------------------------------------------------------------------
```

```
      CFB = 0.D+00
      CUB = 0.D+00
      CVB = 0.D+00
      CZB = 0.D+00
      CPB = 0.D+00
      CAMB = 0.D+00
      CFVB = 0.D+00
      CUSB = 0.D+00
      CFPB = 0.D+00
      CUZB = 0.D+00
      CDBV = 0.D+00
      CDBZP = 0.D+00
      CRB = 0.D+00
      CRZB = 0.D+00
      ELSE
      CFB = ( F(J,1) + F(J-1,1) )/2.D+00
      CUB = ( U(J,1) + U(J-1,1) )/2.D+00
      CVB = ( V(J,1) + V(J-1,1) )/2.D+00
      CZB = ( Z(J,1) + Z(J-1,1) )/2.D+00
      CPB = ( P(J,1) + P(J-1,1) )/2.D+00
      CAMB = ( AM(J,1) + AM(J-1,1) )/2.D+00
      CFVB = ( F(J,1)*V(J,1) + F(J-1,1)*V(J-1,1) )/2.D+00
      CUSB = ( U(J,1)*U(J,1) + U(J-1,1)*U(J-1,1) )/2.D+00
      CFPB = ( F(J,1)*P(J,1) + F(J-1,1)*P(J-1,1) )/2.D+00
      CUZB = ( U(J,1)*Z(J,1) + U(J-1,1)*Z(J-1,1) )/2.D+00
      CDBV = ( B(J,1)*V(J,1) - B(J-1,1)*V(J-1,1) )/DETA(J-1)
      CDBZP = ( BZ(J,1)*P(J,1) - BZ(J-1,1)*P(J-1,1) )/DETA(J-1)
      CLB = CDBV + A1*CFVB - A2*CUSB + CAMB
      CRB = -CLB + CEL*( CFVB - CUSB )
      CLZB = CDBZP + A1Z*CFPB
      CRZB = -CLZB + CEL*( CFPB - CUZB )
      ENDIF
C-----------------------------------------------------------------------------------------------------------------
C     COEFFICIENTS OF THE DIFFERENCED MOMENTUM EQUATION SINCE S7(J)
C     AND S8(J) ARE EQUAL TO 0.5, THEY ARE SPECIFIED WITHOUT VECTOR FORM
C-----------------------------------------------------------------------------------------------------------------
      S1(J) = B(J,2)/DETA(J-1) + ( P1P*F(J,2) - CEL*CFB )/2.D+00
      S2(J) = -B(J-1,2)/DETA(J-1) + ( P1P*F(J-1,2) - CEL*CFB )/2.D+00
      S3(J) = ( P1P*V(J,2) + CEL*CVB )/2.D+00
      S4(J) = ( P1P*V(J-1,2) + CEL*CVB )/2.D+00
      S5(J) = -P2P*U(J,2)
      S6(J) = -P2P*U(J-1,2)
C-----------------------------------------------------------------------
C     COEFFICIENTS OF DIFFERENCED ENERGY EQUATION
C-----------------------------------------------------------------------
      B1(J) = BZ(J,2)/DETA(J-1) + ( P1PZ*F(J,2) - CEL*CFB )/2.D+00
      B2(J) = -BZ(J-1,2)/DETA(J-1) + ( P1PZ*F(J-1,2) - CEL*CFB )/2.D+00
      B3(J) = ( P1PZ*P(J,2) + CEL*CPB )/2.D+00
      B4(J) = ( P1PZ*P(J-1,2) + CEL*CPB )/2.D+00
      B5(J) = CEL*( CZB - Z(J,2) )/2.D+00
      B6(J) = CEL*( CZB - Z(J-1,2) )/2.D+00
      B7(J) = -CEL*( U(J,2) + CUB )/2.D+00
      B8(J) = -CEL*( U(J-1,2) + CUB )/2.D+00
C-----------------------------------------------------------------
C     DEFINITION OF RJ
```

```
C-----------------------------------------------------------------------
      R(1,J) = F(J-1,2) - F(J,2) + DETA(J-1)*UB
      R(2,J) = CRB - ( DBV + P1P*FVB - P2P*USB + CEL*( FB*CVB- CFB*VB ) + AMB )
      R(3,J) = CRZB - ( DBZP + P1PZ*FPB -CEL*(UZB+CUB*ZB-UB*CZB+CFB*PB-FB*CPB ) )
      R(4,J-1) = U(J-1,2) - U(J,2) + DETA(J-1)*VB
      R(5,J-1) = Z(J-1,2) - Z(J,2) + DETA(J-1)*PB
100   CONTINUE
      S7 = 5.D-01
      S8 = 5.D-01
C-----------------------------------------------------------------------
C     SET UP DERIVED BOUNDARY CONDITIONS
C-----------------------------------------------------------------------
      R(1,1) = 0.D+00
      R(2,1) = 0.D+00
      R(3,1) = 0.D+00
      R(4,NPC) = 0.D+00
      R(5,NPC) = 0.D+00
      RETURN
      END
      SUBROUTINE SOLV5
      IMPLICIT REAL*8(A-H,O-Z),INTEGER*4(I-N)
      COMMON /INPT1/ A1,A2,A1Z,ALFA0,ALFA1,IT,IFLAG,GR,RJA,
     1       HPLATE,RADIUS,RKVISI,RE,UINF,RI
      COMMON /ETA3/ ETAE,NP6,NP,DETA(200),ETA(200),A(200),NPC,NNP,NXT,
     1       NX,X(600),CVW,VW(2),VWT
      COMMON /REST4/ F(200,2),U(200,2),V(200,2),Z(200,2),P(200,2),
     1       AM(200,2),B(200,2),BZ(200,2),BT(200)
      COMMON /COEF5/ S1(200),S2(200),S3(200),S4(200),S5(200),S6(200),
     1       S7,S8,B1(200),B2(200),B3(200),B4(200),
     2       B5(200),B6(200),B7(200),B8(200),R(5,200)
      COMMON /SOLV6/ DELF(200),DELU(200),DELV(200),DELZ(200),DELP(200),ABSERR
      DIMENSION A12(200),A13(200),A14(200),A15(200),
     1       A21(200),A22(200),A23(200),A24(200),A25(200),
     2       A31(200),A32(200),A33(200),A34(200),A35(200),
     3       G11(200),G12(200),G13(200),G14(200),G15(200),
     4       G21(200),G22(200),G23(200),G24(200),G25(200),
     5       G31(200),G32(200),G33(200),G34(200),G35(200),
     6       W1(200),W2(200),W3(200),W4(200),W5(200)
C=======================================================================
C     ELEMENTS OF TRIANGLE MATRIX-ALFA FOR J = 0, SET UP SO THAT
C     DELF(1), DELU(1), ALFA0*DELZ(1) + ALFA1*DELO(1) ARE ZERO
C     SINCE A11(J) IS UNITY, IT IS OMITTED
      A12(1) = 0.D+00
      A13(1) = 0.D+00
      A14(1) = 0.D+00
      A15(1) = 0.D+00
      A21(1) = 0.D+00
      A22(1) = 1 D+00
      A23(1) = 0.D+00
      A24(1) = 0.D+00
      A25(1) = 0.D+00
      A31(1) = 0.D+00
      A32(1) = 0.D+00
      A33(1) = 0.D+00
      A34(1) = ALFA0
```

```
      A35(1) = ALFA1
C-----------------------------------------------------------------------
C     ELEMENTS OF W-VECTOR FOR J = 0
C-----------------------------------------------------------------------
      W1(1) = R(1,1)
      W2(1) = R(2,1)
      W3(1) = R(3,1)
      W4(1) = R(4,1)
      W5(1) = R(5,1)
C-----------------------------------------------------------------------
C     FORWARD SWEEP
C-----------------------------------------------------------------------
      DO 100 J = 2,NPC
      AA1 = A(J)*A24(J-1) - A25(J-1)
      AA2 = A(J)*A34(J-1) - A35(J-1)
      AA3 = A(J)*A12(J-1) - A13(J-1)
      AA4 = A(J)*A22(J-1) - A23(J-1)
      AA5 = A(J)*A32(J-1) - A33(J-1)
      AA6 = A(J)*A14(J-1) - A15(J-1)
      AA7 = A(J)*S6(J) - S2(J)
      AA8 = A(J)*S8
      AA9 = A(J)*B6(J)
      AA10 = A(J)*B8(J) - B2(J)
      DET = AA4*AA2 - AA1*AA5 - A21(J-1)*( AA3*AA2 -
     1          AA5*AA6 ) + A31(J-1)*( AA3*AA1 - AA4*AA6 )
C-----------------------------------------------------------------------
C     ELEMENTS OF TRIANGLE MATRIX-GAMMA
C-----------------------------------------------------------------------
      G11(J) = ( AA5*AA1 - AA4*AA2 + A(J)*A(J)*( A21(J-1)*AA2- A31(J-1)*AA1 ) )/DET
      G12(J) = ( AA3*AA2 - AA5*AA6 - A(J)*A(J)*( AA2- A31(J-1)*AA6 ) )/DET
      G13(J) = ( AA4*AA6 - AA3*AA1 + A(J)*A(J)*( AA1- A21(J-1)*AA6 ) )/DET
      G14(J) = G11(J)*A12(J-1) + G12(J)*A22(J-1) + G13(J)*A32(J-1)+ A(J)
      G15(J) = G11(J)*A14(J-1) + G12(J)*A24(J-1) + G13(J)*A34(J-1)
      G21(J) = ( S4(J)*( AA2*AA4 - AA1*AA5 ) + A31(J-1)*( AA1*AA7
     1          - AA4*AA8 ) + A21(J-1)*( AA5*AA8 - AA7*AA2 ) )/DET
      G22(J) = ( AA2*AA7 - AA5*AA8 + A31(J-1)*( AA3*AA8
     1          - AA6*AA7 ) + S4(J)*( AA5*AA6 - AA2*AA3 ) )/DET
      G23(J) = ( AA4*AA8 - AA1*AA7 + S4(J)*( AA3*AA1
     1          - AA4*AA6 ) + A21(J-1)*( AA7*AA6 - AA3*AA8 ) )/DET
      G24(J) = G21(J)*A12(J-1) + G22(J)*A22(J-1) + G23(J)*A32(J-1)- S6(J)
      G25(J) = G21(J)*A14(J-1) + G22(J)*A24(J-1) + G23(J)*A34(J-1)- S8
      G31(J) = ( B4(J)*( AA4*AA2 - AA5*AA1 ) - AA9*( A21(J-1)*AA2
     1          - A31(J-1)*AA1 ) + AA10*( A21(J-1)*AA5- A31(J-1)*AA4 ) )/DET
      G32(J) = ( B4(J)*( AA5*AA6 - AA3*AA2 ) + AA9*( AA2
     1          - A31(J-1)*AA6 ) - AA10*( AA5- A31(J-1)*AA3 ) )/DET
      G33(J) = ( B4(J)*( AA3*AA1 - AA4*AA6 ) - AA9*( AA1
     1          - A21(J-1)*AA6 ) + AA10*( AA4- A21(J-1)*AA3 ) )/DET
      G34(J) = G31(J)*A12(J-1) + G32(J)*A22(J-1) + G33(J)*A32(J-1)- B6(J)
      G35(J) = G31(J)*A14(J-1) + G32(J)*A24(J-1) + G33(J)*A34(J-1)- B8(J)
C-----------------------------------------------------------------------
C     ELEMENTS OF TRIANGLE MATRIX-ALFA
C-----------------------------------------------------------------------
      A12(J) = -A(J) - G14(J)
      A13(J) = A(J)*G14(J)
      A14(J) = -G15(J)
```

```
      A15(J) = A(J)*G15(J)
      A21(J) = S3(J)
      A22(J) = S5(J) - G24(J)
      A23(J) = A(J)*G24(J) + S1(J)
      A24(J) = S7 - G25(J)
      A25(J) = A(J)*G25(J)
      A31(J) = B3(J)
      A32(J) = B5(J) - G34(J)
      A33(J) = A(J)*G34(J)
      A34(J) = B7(J) - G35(J)
      A35(J) = A(J)*G35(J) + B1(J)
C-----------------------------------------------------------------------
C     ELEMENTS OF W-VECTOR
C-----------------------------------------------------------------------
      W1(J) = R(1,J) - G11(J)*W1(J-1) - G12(J)*W2(J-1)
     1        - G13(J)*W3(J-1) - G14(J)*W4(J-1) - G15(J)*W5(J-1)
      W2(J) = R(2,J) - G21(J)*W1(J-1) - G22(J)*W2(J-1)
     1        - G23(J)*W3(J-1) - G24(J)*W4(J-1) - G25(J)*W5(J-1)
      W3(J) = R(3,J) - G31(J)*W1(J-1) - G32(J)*W2(J-1)
     1        - G33(J)*W3(J-1) - G34(J)*W4(J-1) - G35(J)*W5(J-1)
      W4(J) = R(4,J)
      W5(J) = R(5,J)
100   CONTINUE
C-----------------------------------------------------------------------
C     BACKWARD SWEEP
C-----------------------------------------------------------------------
      D1 = A31(NPC)*( A23(NPC)*A15(NPC) - A13(NPC)*A25(NPC) ) +
     1        A33(NPC)*( A25(NPC) - A21(NPC)*A15(NPC) ) -
     2        A35(NPC)*( A23(NPC) - A21(NPC)*A13(NPC) )
      DF = A35(NPC)*( A13(NPC)*W2(NPC) - A23(NPC)*W1(NPC) ) + A33(NPC)*
     1        ( A25(NPC)*W1(NPC) - A15(NPC)*W2(NPC) ) - W3(NPC)*
     2        ( A13(NPC)*A25(NPC) - A23(NPC)*A15(NPC) )
      DV = A31(NPC)*( A15(NPC)*W2(NPC) - A25(NPC)*W1(NPC) ) - A35(NPC)*
     1        ( W2(NPC) - A21(NPC)*W1(NPC) ) + W3(NPC)*
     2        ( A25(NPC) - A15(NPC)*A21(NPC) )
      DP = A31(NPC)*( A23(NPC)*W1(NPC) - A13(NPC)*W2(NPC) ) + A32(NPC)*
     1        ( W2(NPC) - A21(NPC)*W1(NPC) ) - W3(NPC)*(A23(NPC) - A13(NPC)*A21(NPC))
C-----------------------------------------------------------------------
C     ELEMENTS OF DELTA-VECTOR FOR J = NP
C-----------------------------------------------------------------------
      DELF(NPC) = DF/D1
      DELU(NPC) = 0.D+00
      DELV(NPC) = DV/D1
      DELZ(NPC) = 0.D+00
      DELP(NPC) = DP/D1
      DO 200 J = NPC-1,1,-1
      BB1 = DELU(J+1) -A(J+1)*DELV(J+1) - W4(J)
      BB2 = DELZ(J+1) -A(J+1)*DELP(J+1) - W5(J)
      CC1 = W1(J) - A12(J)*BB1 - A14(J)*BB2
      CC2 = W2(J) - A22(J)*BB1 - A24(J)*BB2
      CC3 = W3(J) - A32(J)*BB1 - A34(J)*BB2
      DD1 = A13(J) - A(J+1)*A12(J)
      DD2 = A23(J) - A(J+1)*A22(J)
      DD3 = A33(J) - A(J+1)*A32(J)
      EE1 = A15(J) - A(J+1)*A14(J)
```

```
      EE2 = A25(J) - A(J+1)*A24(J)
      EE3 = A35(J) - A(J+1)*A34(J)
      DETT = DD2*EE3 + A21(J)*DD3*EE1 + A31(J)*DD1*EE2
     1          - A31(J)*DD2*EE1 - A21(J)*DD1*EE3 - DD3*EE2
C-----------------------------------------------------------------------
C     ELEMENTS OF DELTA-VECTOR
C-----------------------------------------------------------------------
      DELF(J) = ( CC1*DD2*EE3 + CC2*DD3*EE1 + CC3*DD1*EE2 -
     1          CC3*DD2*EE1 - CC2*DD1*EE3 - CC1*DD3*EE2 )/DETT
      DELV(J) = ( CC2*EE3 + A21(J)*CC3*EE1 + A31(J)*CC1*EE2
     1          - A31(J)*CC2*EE1 - A21(J)*CC1*EE3 - CC3*EE2 )/DETT
      DELU(J) = BB1 - A(J+1)*DELV(J)
      DELP(J) = ( CC3*DD2 + A21(J)*CC1*DD3 + A31(J)*CC2*DD1
     1          - A31(J)*CC1*DD2 - A21(J)*CC3*DD1 - CC2*DD3 )/DETT
      DELZ(J) = BB2 - A(J+1)*DELP(J)
200   CONTINUE
C-----------------------------------------------------------------------
C     NEW VALUES OF F,U,V,Z,P WITH UNDER-RELAXATION
C-----------------------------------------------------------------------
      ABSERR = 0.D+00
      DO 300 J = 1,NPC
      F(J,2) = F(J,2) + DELF(J)/1.2D+00
      U(J,2) = U(J,2) + DELU(J)/1.2D+00
      V(J,2) = V(J,2) + DELV(J)/1.2D+00
      Z(J,2) = Z(J,2) + DELZ(J)/1.2D+00
      P(J,2) = P(J,2) + DELP(J)/1.2D+00
      IF( Z(J,2) .LT. 0.D+00 ) THEN
      Z(J,2) = 0.D+00
      ENDIF
      ABSERR = ABSERR + DABS( DELF(J) ) + DABS( DELU(J) ) +
     1          DABS( DELV(J) ) + DABS( DELZ(J) ) + DABS( DELP(J) )
300   CONTINUE
C-----------------------------------------------------------------------
C     RESET BOUNDARY CONDITIONS TO AVOID TRUNCATION ERROR
C-----------------------------------------------------------------------
      U(1,2) = 0.D+00
      Z(1,2) = ( 1.D+00 - ALFA1*P(1,2) )/ALFA0
      RETURN
      END
      SUBROUTINE INUPD
      IMPLICIT REAL*8(A-H,O-Z),INTEGER*4(I-N)
      COMMON /INPT1/ A1,A2,A1Z,ALFA0,ALFA1,IT,IFLAG,GR,RJA,
     1          HPLATE,RADIUS,RKVISI,RE,UINF,RI
      COMMON /EOS2/ ZMF(101),RHO(101),TEP(101),RHOM(200),TEMP(200),
     1          DVC(101),PR(101),DVCM(200),PRM(200),JC
      COMMON /ETA3/ ETAE,NP6,NP,DETA(200),ETA(200),A(200),NPC,NNP,NXT,
     1          NX,X(600),CVW,VW(2),VWT
      COMMON /REST4/ F(200,2),U(200,2),V(200,2),Z(200,2),P(200,2),
     1          AM(200,2),B(200,2),BZ(200,2),BT(200)
C=======================================================================
      IF( IFLAG .EQ. 0 ) THEN
      NPC = NP6
      ELSE
      NPC = NP
      ENDIF
```

```
C-----------------------------------------------------------------------
C       SET UP CURVATURE EFFECTS
C-----------------------------------------------------------------------
C       CURVAT = 2.D+00**1.5D+00*HPLATE/RADIUS*( X(NX)/GR )**2.5D-01
        CURVAT = 2.D+00**1.5D+00*HPLATE/RADIUS*( X(NX)/RE )**5.0D-01
C       CURVAT = 0.D+00
        RHOM(1) = RHO(101)
        TEMP(1) = TEP(101)
        AM(1,2) = 1.D+00
        BT(1) = 1.D+00
        B(1,2) = BT(1)*RHOM(1)*DVC(101)/RHO(1)/DVC(1)
        BZ(1,2) = B(1,2)/PR(101)
        DO 100 JC = 2,NPC
        CALL SOURCE
        AM(JC,2) = ( RHO(1)/RHOM(JC) - 1.D+00 )/( RHO(1)/
     1          RHO(101) - 1.D+00 ) * 2.D+00*X(NX)*RI
C       AM(JC,2) = 0.D+00 INVOKE FOR FORCED CONVECTION**
        BT(JC) = BT(JC-1) + CURVAT*RHO(1)/2.D+00*( 1.D+00/RHOM(JC)
     1          + 1.D+00/RHOM(JC-1) )*( ETA(JC) - ETA(JC-1) )
        B(JC,2) = BT(JC)*RHOM(JC)*DVCM(JC)/RHO(1)/DVC(1)
        BZ(JC,2) = B(JC,2)/PRM(JC)
100     CONTINUE
        RETURN
        END
        SUBROUTINE SOURCE
        IMPLICIT REAL*8(A-H,O-Z),INTEGER*4(I-N)
        COMMON /EOS2/ ZMF(101),RHO(101),TEP(101),RHOM(200),TEMP(200),
     1          DVC(101),PR(101),DVCM(200),PRM(200),JC
        COMMON /REST4/ F(200,2),U(200,2),V(200,2),Z(200,2),P(200,2),
     1          AM(200,2),B(200,2),BZ(200,2),BT(200)
C=======================================================================
        DO 10 I = 1,100
        IF( ( Z(JC,2) .GE. ZMF(I) ) .AND. ( Z(JC,2) .LT. ZMF(I+1) ) ) THEN
        RHOM(JC) = RHO(I) + ( RHO(I+1) - RHO(I) )*( Z(JC,2) -
     1          ZMF(I) )/( ZMF(I+1) - ZMF(I) )
        TEMP(JC) = TEP(I) + ( TEP(I+1) - TEP(I) )*( Z(JC,2) -
     1          ZMF(I) )/( ZMF(I+1) - ZMF(I) )
        DVCM(JC) = DVC(I) + ( DVC(I+1) - DVC(I) )*( Z(JC,2) -
     1          ZMF(I) )/( ZMF(I+1) - ZMF(I) )
        PRM(JC) = PR(I) + ( PR(I+1) - PR(I) )*( Z(JC,2) -
     1          ZMF(I) )/( ZMF(I+1) - ZMF(I) )
        ENDIF
10      CONTINUE
        RETURN
        END
        SUBROUTINE GROWTH
        IMPLICIT REAL*8(A-H,O-Z),INTEGER*4(I-N)
        COMMON /ETA3/ ETAE,NP6,NP,DETA(200),ETA(200),A(200),NPC,NNP,NXT,
     1          NX,X(600),CVW,VW(2),VWT
        COMMON /REST4/ F(200,2),U(200,2),V(200,2),Z(200,2),P(200,2),
     1          AM(200,2),B(200,2),BZ(200,2),BT(200)
C=======================================================================
        NNP = 3
        NP0 = NP
        NP1 = NP + 1
```

```
      NP = NP + NNP
      IF( NP .GT. 310 ) THEN
      NP = 400
      ENDIF
      DO 100 L = 1,2
      DO 101 J = NP1,NP
      DETA(J) = DETA(J-1)
      A(J) = A(J-1)
      ETA(J) = ETA(J-1) + DETA(J)
      F(J,L) = F(NP0,L) + U(NP0,L)*( ETA(J) - ETA(J -1) )
      U(J,L) = U(NP0,L)
      V(J,L) = V(NP0,L)
      Z(J,L) = Z(NP0,L)
      P(J,L) = P(NP0,L)
      AM(J,L) = AM(NP0,L)
      B(J,L) = B(NP0,L)
      BZ(J,L) = BZ(NP0,L)
101   CONTINUE
100   CONTINUE
      RETURN
      END
      SUBROUTINE OUTPUT
      IMPLICIT REAL*8(A-H,O-Z),INTEGER*4(I-N)
      COMMON /INPT1/ A1,A2,A1Z,ALFA0,ALFA1,IT,IFLAG,GR,RJA,
     1        HPLATE,RADIUS,RKVISI,RE,UINF,RI
      COMMON /EOS2/ ZMF(101),RHO(101),TEP(101),RHOM(200),TEMP(200),
     1        DVC(101),PR(101),DVCM(200),PRM(200),JC
      COMMON /ETA3/ ETAE,NP6,NP,DETA(200),ETA(200),A(200),NPC,NNP,NXT,
     1        NX,X(600),CVW,VW(2),VWT
      COMMON /REST4/ F(200,2),U(200,2),V(200,2),Z(200,2),P(200,2),
     1        AM(200,2),B(200,2),BZ(200,2),BT(200)
      DIMENSION Y(200)
C=====================================================================
      IDNP = 1
      NDX1 = 1
C---------------------------------------------------------------------
C     OUTPUT CONTROL (ADD OR DELETE COMMENTS FOR DESIRED OUTPUT)
C---------------------------------------------------------------------
      IF( (NX .LT. NXT) .AND. (NX .NE. 1) ) THEN
      NDX = NDX1
      NX1 = NX + 1
      IPRINT = NX1/NDX - NX/NDX
      IF( IPRINT .EQ. 0 ) GO TO 10
      ENDIF
C*********************************************************************
C     WRITE(6,1000) NX,X(NX),VW(2)
      1000 FORMAT(1H0,4HNX =,I3,5X,3HX =,F10.7,5X,4HVW =,E10.4)
      RMBR = RHOM(1)*VW(2)
C     WRITE(6,2000) RE,RJA,RMBR
2000  FORMAT(1H0,4HRE =,E10.4,5X,4HJA =,E10.4,5X,5HMBR =,E10.4)
      WRITE(6,2050) X(NX),RMBR
2050  FORMAT(1H0,F10.7,T20,F15.10)
C     WRITE(6,3000)
3000   FORMAT(1H0,2X,1HJ,3X,3HETA,4X,1HF,9X,2HF1,8X,2HF2,8X,1HZ,9X,2HZ1)
C     WRITE(6,4000) ( J,ETA(J),F(J,2),U(J,2),V(J,2),Z(J,2),P(J,2)J = 1,NP,IDNP )
```

```
C       WRITE(6,4050) X(NX),RMBR,P(1,2)
4050    FORMAT(1H0,F10.7,T20,F15.10,T40,F15.10)
C*****************************************************************************
C       WRITE(6,4000) NP,ETA(NP),F(NP,2),U(NP,2),V(NP,2),Z(NP,2),P(NP,2)
C       WRITE(6,4100) NP,ETA(NP),F(NP,2),U(NP,2),V(NP,2)
4100    FORMAT(I3,F7.2,3F10.5)
4000    FORMAT(1H0,I3,F7.2,5F10.5)
C-----------------------------------------------------------------------
C       UPDATE PROFILES
C-----------------------------------------------------------------------
        PX = HPLATE*X(NX)
C       WRITE(6,5000) PX
5000    FORMAT(1H0,'PX =',E15.8)
        10 DO 100 J = 1,NP
        F(J,1) = F(J,2)
        U(J,1) = U(J,2)
        V(J,1) = V(J,2)
        Z(J,1) = Z(J,2)
        P(J,1) = P(J,2)
        B(J,1) = B(J,2)
        BZ(J,1) = BZ(J,2)
        AM(J,1) = AM(J,2)
C-----------------------------------------------------------------------------------------------
C       TRANSFORM DIMENSIONLESS VARIABLE TO PHYSICAL LENGTH
C-----------------------------------------------------------------------------------------------
        Y(J) = RADIUS*( DSQRT( BT(J) ) - 1.D+00 )
        UP = DSQRT( 4.D+00*9.80665D+00*( RHOM(NP)/RHOM(1) - 1.D+00 )
      1          *X(NX)*HPLATE )*U(J,2)
C       IF( (NX .NE. 1) .AND. (IPRINT .NE. 0) .OR. (NX .EQ. NXT) ) THEN
C       IF( J .EQ. 1 ) THEN
C       ETAFP = 0.D+00
C       ELSE
C       ETAFP = ETAFP + ( GR/X(NX) )**2.5D-01/HPLATE/RHOM(NP)
C     1          /2.D+00*( RHOM(J) + RHOM(J-1) )*( Y(J) - Y(J-1) )/DSQRT( 2.D+00 )
C       ENDIF
C       WRITE(6,6000) ETAFP,Z(J,2)
6000    FORMAT(1H0,F15.6,5X,F15.6)
C       ENDIF
C       WRITE(6,7000) Y(J),F(J,2),UP,TEMP(J)
7000    FORMAT(1H0,4F15.6)
C       WRITE(6,8000) Y(J),Z(J,2)
8000    FORMAT(1H0,2F15.6)
100     CONTINUE
        NX = NX + 1
C-----------------------------------------------------------------------------------------------
C       INITIALIZE WALL STREAM FUNCTION DUE TO WALL BLOWING EFFECTS
C-----------------------------------------------------------------------------------------------
C       CVW = -HPLATE/RKVISI/DSQRT( 8.D+00 )*RHO(101)/RHO(1)/GR**2.5D-01
        CVW = -DSQRT(2.D+00)/2.D+00*(HPLATE*RHO(101)/DVC(1))/RE**0.5D+00
        F(1,2) = F(1,1)*( X(NX-1)/X(NX) )**5.0D-01
      1          + CVW*( VW(1) + VW(2) )/2.D+00*( X(NX) - X(NX - 1) )/X(NX)**5.0D-01
        RETURN
        END
```

Table A-1. Data for state relationships used in flow calculations: temperature (T), density (ρ), viscosity (μ), and Prandtl number (Pr) as functions of conserved scalar (Z).

Z	T (K)	ρ (kg/m^3)	μ (kg/m-s)	Pr
0.0000	298.2	5.9696E-01	1.5573E-05	0.7484
0.0100	685.1	2.5784E-01	3.1761E-05	0.7444
0.0200	1002.1	1.7726E-01	4.2585E-05	0.7466
0.0300	1228.2	1.4475E-01	4.9860E-05	0.7448
0.0400	1388.1	1.2070E-01	5.5290E-05	0.7605
0.0500	1454.7	1.0348E-01	5.8402E-05	0.7864
0.0600	1492.2	9.0196E-02	6.0575E-05	0.8088
0.0700	1517.7	7.9616E-02	6.2141E-05	0.8258
0.0800	1537.2	7.0993E-02	6.3211E-05	0.8378
0.0900	1553.2	6.3821E-02	6.3839E-05	0.8460
0.1000	1567.1	5.7741E-02	6.4050E-05	0.8513
0.1100	1580.5	5.2516E-02	6.3883E-05	0.8549
0.1200	1608.6	4.8224E-02	6.3751E-05	0.8616
0.1300	1644.6	4.4299E-02	6.2848E-05	0.8664
0.1400	1681.9	4.0843E-02	6.1308E-05	0.8674
0.1500	1711.6	3.7935E-02	5.9710E-05	0.8643
0.1600	1735.9	3.5437E-02	5.8213E-05	0.8583
0.1700	1757.2	3.3242E-02	5.6813E-05	0.8507
0.1800	1777.1	3.1282E-02	5.5498E-05	0.8418
0.1900	1796.4	2.9512E-02	5.4258E-05	0.8321
0.2000	1816.2	2.7895E-02	5.3092E-05	0.8219
0.2100	1837.5	2.6400E-02	5.2002E-05	0.8113
0.2200	1861.9	2.4998E-02	5.0992E-05	0.8006
0.2300	1892.1	2.3652E-02	5.0092E-05	0.7879
0.2400	1933.3	2.2324E-02	4.9367E-05	0.7790
0.2500	1989.1	2.1016E-02	4.8916E-05	0.7689
0.2600	2045.0	1.9871E-02	4.8576E-05	0.7597
0.2700	2089.0	1.8932E-02	4.8117E-05	0.7510
0.2800	2125.2	1.8114E-02	4.7582E-05	0.7426
0.2900	2159.3	1.7371E-02	4.7034E-05	0.7343
0.3000	2193.1	1.6674E-02	4.6523E-05	0.7262
0.3100	2229.8	1.6005E-02	4.6095E-05	0.7186
0.3200	2273.0	1.5342E-02	4.5806E-05	0.7114
0.3300	2330.0	1.4657E-02	4.5769E-05	0.7048
0.3400	2415.6	1.3895E-02	4.6242E-05	0.6997
0.3500	2541.7	1.3048E-02	4.7426E-05	0.6972
0.3600	2685.4	1.2242E-02	4.8919E-05	0.6969
0.3700	2827.4	1.1538E-02	5.0371E-05	0.6977
0.3800	2961.2	1.0939E-02	5.1719E-05	0.6988
0.3900	3062.0	1.0499E-02	5.2666E-05	0.7002
0.4000	3111.1	1.0236E-02	5.2969E-05	0.7016
0.4100	3119.2	1.0095E-02	5.2751E-05	0.7030
0.4200	3097.5	1.0040E-02	5.2164E-05	0.7042
0.4300	3053.9	1.0048E-02	5.1308E-05	0.7052
0.4400	2997.4	1.0100E-02	5.0313E-05	0.7058

Table A-1 -- continued

0.4500	2938.2	1.0170E-02	4.9332E-05	0.7063
0.4600	2884.1	1.0236E-02	4.8482E-05	0.7069
0.4700	2838.8	1.0288E-02	4.7819E-05	0.7079
0.4800	2802.1	1.0321E-02	4.7338E-05	0.7092
0.4900	2772.6	1.0340E-02	4.7007E-05	0.7109
0.5000	2748.4	1.0346E-02	4.6788E-05	0.7129
0.5100	2728.1	1.0344E-02	4.6648E-05	0.7152
0.5200	2710.5	1.0336E-02	4.6565E-05	0.7176
0.5300	2694.8	1.0324E-02	4.6520E-05	0.7201
0.5400	2680.3	1.0309E-02	4.6499E-05	0.7227
0.5500	2666.6	1.0293E-02	4.6495E-05	0.7254
0.5600	2653.2	1.0276E-02	4.6497E-05	0.7281
0.5700	2639.7	1.0261E-02	4.6496E-05	0.7309
0.5800	2625.6	1.0247E-02	4.6481E-05	0.7336
0.5900	2610.5	1.0238E-02	4.6442E-05	0.7362
0.6000	2593.5	1.0234E-02	4.6363E-05	0.7387
0.6100	2573.4	1.0240E-02	4.6216E-05	0.7411
0.6200	2548.0	1.0263E-02	4.5959E-05	0.7433
0.6300	2513.0	1.0316E-02	4.5504E-05	0.7451
0.6400	2459.7	1.0431E-02	4.4671E-05	0.7461
0.6500	2375.5	1.0658E-02	4.3217E-05	0.7460
0.6600	2267.5	1.0997E-02	4.1296E-05	0.7452
0.6700	2159.3	1.1377E-02	3.9400E-05	0.7448
0.6800	2063.1	1.1753E-02	3.7799E-05	0.7454
0.6900	1982.8	1.2096E-02	3.6584E-05	0.7474
0.7000	1917.8	1.2395E-02	3.5741E-05	0.7506
0.7100	1864.9	1.2654E-02	3.5193E-05	0.7550
0.7200	1820.7	1.2881E-02	3.4857E-05	0.7601
0.7300	1782.7	1.3086E-02	3.4669E-05	0.7657
0.7400	1748.9	1.3275E-02	3.4581E-05	0.7718
0.7500	1718.1	1.3454E-02	3.4563E-05	0.7782
0.7600	1689.3	1.3628E-02	3.4590E-05	0.7848
0.7700	1662.0	1.3800E-02	3.4645E-05	0.7916
0.7800	1635.5	1.3972E-02	3.4713E-05	0.7985
0.7900	1609.6	1.4148E-02	3.4781E-05	0.8056
0.8000	1583.8	1.4331E-02	3.4838E-05	0.8127
0.8100	1573.2	1.4384E-02	3.4304E-05	0.8110
0.8200	1562.1	1.4442E-02	3.3771E-05	0.8094
0.8300	1550.1	1.4511E-02	3.3258E-05	0.8083
0.8400	1539.0	1.4588E-02	3.2700E-05	0.8061
0.8500	1532.9	1.4657E-02	3.1937E-05	0.7995
0.8600	1526.4	1.4729E-02	3.1148E-05	0.7927
0.8700	1519.6	1.4806E-02	3.0333E-05	0.7856
0.8800	1512.3	1.4888E-02	2.9491E-05	0.7782
0.8900	1504.4	1.4976E-02	2.8623E-05	0.7706
0.9000	1496.0	1.5070E-02	2.7728E-05	0.7627
0.9100	1486.8	1.5172E-02	2.6807E-05	0.7547
0.9200	1476.8	1.5284E-02	2.5862E-05	0.7467
0.9300	1465.9	1.5406E-02	2.4893E-05	0.7385
0.9400	1453.7	1.5542E-02	2.3906E-05	0.7305
0.9500	1440.2	1.5696E-02	2.2904E-05	0.7225
0.9600	1425.0	1.5872E-02	2.1896E-05	0.7149

Table A-1 -- continued

0.9700	1407.8	1.6075E-02	2.0894E-05	0.7078
0.9800	1388.2	1.6315E-02	1.9914E-05	0.7014
0.9900	1365.8	1.6602E-02	1.8979E-05	0.6960
1.0000	1340.5	1.6946E-02	1.8120E-05	0.6920

APPENDIX B

SUFFICIENT AND NECESSARY CONDITION FOR SIMILARITY SOLUTIONS

To obtain a sufficient and necessary condition for similarity solutions, the nonsimilar terms of the right-hand sides of the momentum and mixture fraction equations, Eqs. (2.30) and (2.38), are examined. First, the nonsimilar term in Eq. (2.30) is set equal to zero.

$$\frac{\partial f'}{\partial \xi} f - \frac{\partial f}{\partial \xi} f'' = 0 \tag{B.1}$$

The dimensionless stream function, f, is assumed to consist of two parts using separation of variables.

$$f = X(\xi)H(\eta) \tag{B.2}$$

Substituting into Eq. (B.1), one obtains

$$XX'(H'^2 - HH'') = 0 \tag{B.3}$$

Three possibilities exist for Eq. (B.3), $X = 0$, $X' = 0$, or $H'^2 - HH'' = 0$. The condition of $X = 0$ leads to trivial solution and is excluded from further consideration. The solution to $H'^2 - HH'' = 0$ is obtained:

$$H = c_1 EXP(c_2 \eta) \tag{B.4}$$

The boundary conditions, Eq. (2.39), are required to obtain solution to Eq. (B.4). The boundary conditions are as follows:

$$X(\xi)H(0) = f_w = A\xi^{-1/2} \int_0^{\xi} v_w(\xi) d\xi$$

where $A = -\frac{\sqrt{2}}{2} \frac{\rho_w H}{\mu_\infty} \frac{1}{Re^{1/2}}$,

with

$$H'(0) = 0 \qquad H'(\infty) = 1 \tag{B.5}$$

Equation (B.4) subject to the boundary conditions of Eq. (B.5) also leads to a trivial solution.

Finally, $X' = 0$ is satisfied if X = constant or v_w is proportional to $\xi^{-1/2}$. The dimensionless stream function is a function of η only, implying similarity solutions for momentum equation.

To complete the necessary condition, the nonsimilar term of Eq. (2.38) is set to zero. Separation of variables for mixture fraction is employed.

$$\frac{\partial Z}{\partial \xi} f' - \frac{\partial f}{\partial \xi} Z' = 0 \tag{B.6}$$

$$Z = X_1(\xi)\, H_1(\eta) \tag{B.7}$$